Forced solitary waves and hydraulic falls in two-layer flows

By SAMUEL SHAN-PU SHEN†

Department of Mathematics, University of Saskatchewan, Saskatoon, Canada S7N 0W0

Long nonlinear waves in the two-layer flow of an inviscid, incompressible fluid are considered. Both the free surface and the interface of the two fluids are unknown free boundaries. The flow is forced by an obstruction on the bottom and/or an external pressure (usually called the wind stress) on the free surface. Away from the critical depth ratio between the surface layer and the internal layer of the fluids, the weak nonlinearity is of second order. Then there exists a balance between the dispersion and the second-order nonlinearity. The first-order asymptotic approximations of both free-surface elevation and interface elevation satisfy forced Korteweg–de Vries equations (fKdV). Because of the existence of two modes, the total number of types of solutions is double that for the single-layer flow. There are two hydraulic falls and four solitary waves for positive forcing. The first hydraulic fall and the first two solitary waves correspond to the fast mode. The remaining ones correspond to the slow mode. The first hydraulic fall was numerically found by Forbes (1989) by directly integrating the Laplace equation with nonlinear boundary conditions. There are two types of forcing according to the length of the base of the obstruction. One type is called local and the length of its base has the same scale as the height of the forcing. The expression of the forcing in the fKdV is given by the Dirac delta function. Based upon our long-wave scale the horizontal laboratory lengthscale is shrunk by $\epsilon^{\frac{1}{2}}$, while the vertical laboratory lengthscale is unchanged. Hence the semicircular bumps in the papers by Vanden-Broeck (1987), and Forbes (1988, 1989) are all considered to be local in the present paper. For the locally forced cases, stationary problems have been solved analytically. We have derived analytical expressions for the upstream speeds U_L and U_C, at which the hydraulic falls can occur and solitary waves respectively cease to exist. The formulae are reduced to those due to Miles (1986) in the case of a single-layer flow and very small forcing. A full comparison among the asymptotic, computational and experimental results is provided. The comparison shows that the difference is less than 10% for U_L and U_C in most of the parameter range where the asymptotic method is valid, the computational scheme converges and experiments were conducted (see figure 10). The second type of forcing is called non-local and the length of the base of the obstruction has the same scale as the wavelength. The existence and behaviour of the stationary solutions of the non-locally forced fKdV are described. Surprisingly, there can be more than four solitary waves sustained on the site of some negative forcing.

---

† Current address: Applied Mathematics Institute and Department of Mathematics, University of Alberta, Edmonton, Canada T6G 2G1.

S. S. Shen

1. Introduction

There has been an increasing interest in studying the forced long nonlinear waves in fluid flows since the innovative experiments of Huang *et al.* (1982) and the remarkable numerical findings of Wu & Wu (1982). Their studies are on forced waves in a current of near critical speed of shallow water flows. The forcing is due to a bottom obstruction and/or an external surface pressure. New findings for a single-layer flow in the last decade include upstream periodically radiated solitons (Wu & Wu 1982), multiple solitary waves (Vanden-Broeck 1987) and hydraulic falls (Sivakumaran, Tingsanchali & Hosking 1983). These phenomena do not exist in unforced channel flows. There are numerous published papers that elucidate these conspicuous phenomena from various perspectives. The published studies may be classified into three categories: experimental approach (Huang *et al.* 1982; Sivakumaran *et al.* 1983; Forbes 1988), computational approach (Forbes & Schwartz 1982; Vanden-Broeck 1987; Forbes 1988, 1989) and asymptotic approach (Wu & Wu 1982; Miles 1986; Mei 1986; Naghdi & Vongsarnpigoon 1986; Shen 1989). Here we have listed only a few among many excellent contributions. The published results for single-layer flows can be summarized as follows.

For a two-dimensional channel, there are two important values of the Froude number, which is the ratio of the upstream uniform velocity to the critical speed of shallow water waves, $F_C > 1$ and $F_L < 1$ such that: (i) when $F \geqslant F_C$, there are two stationary solitary waves sustained over the site of the forcing, and at $F = F_C$ the two solitary waves merge into one; (ii) when $F < F_L$, there is a unique stationary downstream cnoidal wave matched with the upstream null solution; (iii) when $F = F_L$, the period of the cnoidal wave extends to infinity and the solution becomes a hydraulic fall; (iv) for some values of F in the interval (F_L, F_C), solitons are periodically generated at the site of forcing and radiated upstream. In this case, the flow never approaches a steady state.

In the above, F_C is called the turning point and F_L the cutoff point. These terms come from bifurcation theory. The multiple solitary wave solutions are called supercritical solitary waves. The downstream cnoidal wave solution is called a subcritical cnoidal wave. The soliton radiation region of the Froude number is called the transcritical range. In the past, one major effort in this area of research was to determine the values of F_C and F_L. The existence of the two values was conjectured in Wu & Wu (1982), and approximate values were first found by Miles (1986) by an asymptotic method. The exact value for F_C was first found by Vanden-Broeck (1987) and that for F_L by Forbes (1988) by direct numerical integration of the Laplace equation. We refer to this direct numerical integration of the Laplace equation as the computational method in the present paper.

To obtain the aforementioned results, experiments were conducted for forcing by a semicircular bottom obstruction type (Huang *et al.* 1982; Forbes 1988) and by a Gaussian bottom obstruction type (Sivakumaran *et al.* 1983). Direct numerical integrations were performed for bottom obstructions of a semicircle (Forbes & Schwartz 1982), a rectangular step (King & Blohr 1987), a triangle (Dias & Vanden-Broeck 1989) and a Gaussian distribution (King & Blohr 1990). Asymptotic methods can include the wind stress type of forcing very easily. Although the complication of the shape of the distributed forcing causes major difficulties for the computational method, it poses almost no problem in the asymptotic approach. Further, the long-wave asymptotic method has been systematically extended to flows in channels of arbitrary cross-sections (Shen 1989). Shen recently showed that, for the locally

forced case, the surface waves are independent of the shape of the bottom obstruction, but instead are dependent only on its area (Shen 1991).

It is even more important to study the forced near-critical waves in stratified flows for meteorological and oceanographic reasons. It is a common feature that atmospheric and oceanic currents are stratified at near critical speeds (Baines 1987; Patoine & Warn 1982). In §5, it will be seen that this 'near' does not preclude reasonably large intervals which include the critical speeds. Hence the assumption of 'near' critical speed will not pose much constraint on applications of the asymptotic theory to practical problems. Asymptotic studies on forced stratified flows were first conducted by Grimshaw & Smyth (1986). Extensive experimental work on two-layer flows was conducted by Baines (1984), and was followed by that of Melville & Helfrich (1987). The latter only takes into account the interface as the free boundary. The upper surface is rigidly covered. Besides the time-honoured phenomena such as soliton radiation etc, some new phenomena were discovered such as dispersive and non-dissipative internal bores, the existence of the critical layer and the appearance of third-order nonlinearity. The clever direct numerical integration scheme for the two-layer flow due to Forbes (1989) recovered a hydraulic fall in the two-layer flow. Despite these works, the studies on weakly nonlinear waves in two-layer flows are far from complete. In the current paper we report our findings in this area of research. They are: (i) analytic expressions for the values of the turning point and the cutoff point of the upstream velocities; (ii) locally forced four solitary waves and non-locally forced six to eight solitary waves; (iii) two hydraulic falls; (iv) agreements of asymptotic results with experimental and computational results for supercritical and subcritical flows.

An asymptotic approach is employed here. The first-order elevation of both the free surface and the interface yield forced Korteweg–de Vries equations (fKdV). There are two modes because of the two-layer stratification. The coefficients of the fKdV depend not only on the flow configuration but also on the modes. The fKdV equations for the free-surface elevation and the interface elevation are decoupled. This is a consequence of the second-order weak nonlinearity. The interplay between the free surface and the interface is not that strong. A detailed comparison among the available data obtained by experiments, direct numerical integrations and our asymptotic method is made. The comparison shows that the difference is less than 10% in most of the parameter range where the asymptotic method is valid, the computational method converges and experiments were conducted. This is a surprisingly good agreement among the results obtained from different approaches. Particularly for the comparison of the analytic results from our asymptotic method with those from both experiments and direct numerical integrations, such a close agreement was unexpected.

The aforementioned comparisons are in the regime of supercritical and subcritical stationary flows. In the regime of transcritical unsteady flow, solitons are periodically generated at the site of forcing and radiated upstream. This phenomenon of periodic soliton generation was observed from numerical solutions of both the fKdV and the forced Boussinesq equations, and also from laboratory experiments by Professor T. Yao-Tsu Wu's group in Caltech. Their numerical solutions were compared with the experimental results and the agreement was good (Lee, Yates & Wu 1989). Similar comparisons were made by Melville & Helfrich (1987) for internal periodic soliton generation.

The plan of the paper is as follows. In §2 we present the details of the derivation of the fKdV equations. Section 3 describes the stationary solitary wave solutions and

the turning point bifurcations for supercritical flows. The turning points are given explicitly for the locally forced case. Here we specify the ratio of the upstream velocity of the surface layer to that of the internal layer. Hence only the upstream velocity of the internal layer is considered as the primary varying parameter. However, the value of the aforementioned ratio is not restricted to be equal to one. In §4, stationary cnoidal wave solutions and hydraulic falls are delineated. The cutoff points for the locally forced case are analytically found. The comparison among the asymptotic, computational and experimental results is given in §5. Section 6 contains discussion and concluding remarks.

2. Derivation of the fKdV equations

The fluids under consideration are inviscid and incompressible. The difference between the two fluids is in the density. To avoid the Helmholtz instability, the density of the surface-layer fluid is less than or equal to the density of the fluid of the internal layer. The ratio of the upstream velocity of the surface layer to that of the internal layer is a constant, denoted by γ. The fluid motion in both layers is assumed to be irrotational. The flow is confined in a two-dimensional channel and forced by a bottom obstruction and/or a wind stress (see figure 1). Let the x^*-axis be aligned along the longitudinal direction and on the bottom of the channel, and the y^*-axis vertically opposite to the gravitational direction. The subscripts 's' and 'i' signify the quantities for surface layer and the internal layer respectively. H_s and H_i are the upstream depths of the two fluids respectively, ρ_s and ρ_i are densities, p^* is pressure, Φ_s^* and Φ_i^* are flow potentials, η_s^* and η_i^* are free boundary elevations, and c_s^* and c_i^* are the upstream uniform velocities; $y^* = h^*(x^*)$ expresses the bottom topography and $p^* = \bar{p}^*$ stands for the wind stress; g is the gravitational acceleration and t^* is time.

Let L be the typical wavelength. We use L and H_i as the horizontal and vertical scales respectively and ρ_i as the density scale. The following dimensionless variables are introduced:

$$\epsilon = (H_i/L)^2 \ll 1 \quad \text{(small parameter in our asymptotic analysis)};$$

$$\sigma = H_s/H_i, \quad \rho = \rho_s/\rho_i \leqslant 1;$$

$$(x, y) = (\epsilon^{\frac{1}{2}}x^*, y^*)/H_i, \quad t = t^*(g/H_i)^{\frac{1}{2}}\epsilon^{\frac{3}{2}};$$

$$\Phi_s = \epsilon^{\frac{1}{2}}\Phi_s^*/[H_i(gH_i)^{\frac{1}{2}}], \quad \Phi_i = \epsilon^{\frac{1}{2}}\Phi_i^*/[H_i(gH_i)^{\frac{1}{2}}];$$

$$p = p^*/(\rho_i gH_i);$$

$$c_s = c_s^*/(gH_i)^{\frac{1}{2}}, \quad c_i = c_i^*/(gH_i)^{\frac{1}{2}};$$

$$\eta_s = \eta_s^*/H_i, \quad \eta_i = \eta_i^*/H_i;$$

$$h(x) = \epsilon^{-2}h^*(x^*)/H_i \quad \text{(small bottom obstruction assumption)};$$

$$\bar{p}(x) = \epsilon^{-2}\bar{p}^*(x^*)/(\rho_i gH_i) \quad \text{(small wind stress assumption)}.$$

In terms of the dimensionless variables, $y = 1 + \sigma + \eta_s$ is the free surface and $y = 1 + \eta_i$ is the interface. It is our intention to investigate the free-surface and interface waves in the near-critical flows. The precise meaning of near-critical velocity is that the upstream uniform velocities c_s and c_i take the forms

$$c_s = c_s^{(0)} + \epsilon\lambda_s, \quad c_i = c_i^{(0)} + \epsilon\lambda_i. \tag{1}$$

Here $c_s^{(0)}$ and $c_i^{(0)}$ are the critical velocities which will be determined by the solvability condition of the second-order perturbation problem. We shall see this later in this
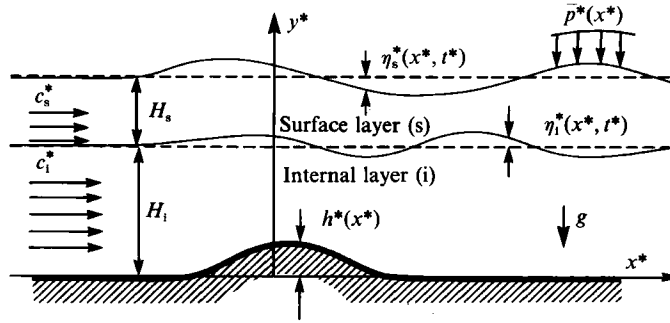
FIGURE 1. Configuration of the two-layer fluid flow forced by a bump and wind stress.

section. λ_s and λ_i are constants which signify the perturbations of the upstream uniform velocities about the corresponding critical velocities.

Then the flow potentials take the forms

$$\Phi_s = c_s x + \phi_s(x, y, t), \quad \Phi_i = c_i x + \phi_i(x, y, t). \tag{2}$$

Hence $\phi_s(x, y, t)$ and $\phi_i(x, y, t)$ are the perturbations of the flow potentials about the upstream uniform flows.

In the fluid domain, the flow potentials both yield the Laplace equation. On the free surface, a kinetic condition and the Bernoulli equation must be satisfied. On the interface, the kinetic condition is that the two fluids do not penetrate into each other, and the dynamic condition is a combined type of Bernoulli equation. On the bottom, a kinetic condition for the internal fluid not penetrating into the rigid bottom should be satisfied. In terms of the dimensionless quantities, the above equations can be written as follows:

$$\epsilon\phi_{s,xx} + \phi_{s,yy} = 0, \quad 1 + \eta_i < y < 1 + \sigma + \eta_s, \tag{3}$$

$$\epsilon\phi_{i,xx} + \phi_{i,yy} = 0, \quad \epsilon^2 h < y < 1 + \eta_i; \tag{4}$$

on the free-surface $y = 1 + \sigma + \eta_s$:

$$\epsilon\eta_{s,t} + (c_s + \phi_{s,x})\eta_{s,x} = \epsilon^{-1}\phi_{s,y}, \tag{5}$$

$$\epsilon\phi_{s,t} + \tfrac{1}{2}(\phi_{s,x}^2 + \epsilon^{-1}\phi_{s,y}^2) + c_s\phi_{s,x} + \eta_s + \epsilon^2\rho^{-1}\bar{p} = 0; \tag{6}$$

on the interface $y = 1 + \eta_i$:

$$\epsilon\eta_{i,t} + (c_s + \phi_{s,x})\eta_{i,x} = \epsilon^{-1}\phi_{s,y}, \tag{7}$$

$$\epsilon\eta_{i,t} + (c_i + \phi_{i,x})\eta_{i,x} = \epsilon^{-1}\phi_{i,y}, \tag{8}$$

$$\rho[\epsilon\phi_{s,t} + \tfrac{1}{2}(\phi_{s,x}^2 + \epsilon^{-1}\phi_{s,y}^2) + c_s\phi_{s,x} + \eta_i] = \epsilon\phi_{i,t} + \tfrac{1}{2}(\phi_{i,x}^2 + \epsilon^{-1}\phi_{i,y}^2) + c_i\phi_{i,x} + \eta_i; \tag{9}$$

and on the bottom $y = \epsilon^2 h(x)$:

$$(c_i + \phi_{i,x})h_{,x} = \epsilon^{-3}\phi_{i,y}. \tag{10}$$

We would like to proceed with the asymptotic expansion in the strips $S_i = \{(x, y) \in \Re^2 \mid 0 \leqslant y \leqslant 1\}$ and $S_s = \{(x, y) \in \Re^2 \mid 1 \leqslant y \leqslant 1 + \sigma\}$. Hence it is required to approximate the boundary conditions on the free surface, the interface and the bottom, so that the boundary conditions are approximately prescribed on $y = 1 + \sigma$, $y = 1$ and $y = 0$ respectively. Here we take the Taylor expansions as the approximations. Therefore, after the approximation, all of the above equations are confined in the two strips S_i and S_s.

It is our intention to study dispersive waves with second-order nonlinearity. Then the response of the free boundaries (here the free surface and the interface) to the

forcing of order ϵ^2 is of order ϵ. We shall see later on that this nonlinearity assumption does not describe the stronger nonlinearity in a neighbourhood of the critical ratio of the depths. In this neighbourhood, the response of the free surface and the interface to a forcing of order ϵ^2 is of order $\epsilon^{\frac{1}{2}}$. Consequently, a third-order nonlinearity is introduced to the asymptotically reduced equation. However, in this paper we concentrate on the second-order nonlinearity. We assume asymptotic expansions for $(\phi_s, \phi_i, \eta_s, \eta_i)$ as follows:

$$\phi_s = \epsilon\phi_s^{(1)}(x, y, t) + \epsilon^2\phi_s^{(2)}(x, y, t) + O(\epsilon^3), \tag{11}$$

$$\phi_i = \epsilon\phi_i^{(1)}(x, y, t) + \epsilon^2\phi_i^{(2)}(x, y, t) + O(\epsilon^3), \tag{12}$$

$$\eta_s = \epsilon\eta_s^{(1)}(x, t) + \epsilon^2\eta_s^{(2)}(x, t) + O(\epsilon^3), \tag{13}$$

$$\eta_i = \epsilon\eta_i^{(1)}(x, t) + \epsilon^2\eta_i^{(2)}(x, t) + O(\epsilon^3). \tag{14}$$

Substitute the above asymptotic expansions into the approximated governing equations on the strips S_s and S_i and consider the problems of the first three orders according to the powers of ϵ.

The first-order problem:

$$\phi_{s,yy}^{(1)} = 0, \quad 1 < y < 1 + \sigma, \tag{15}$$

$$\phi_{i,yy}^{(1)} = 0, \quad 0 < y < 1; \tag{16}$$

$$\left. \begin{array}{r} \phi_{s,y}^{(1)} = 0 \\ \tfrac{1}{2}\phi_{s,y}^{(1)^2} + c_s^{(0)}\,\phi_{s,x}^{(1)} + \eta_s^{(1)} = 0 \end{array} \right\} \quad \text{on } y = 1 + \sigma; \tag{17} \tag{18}$$

$$\left. \begin{array}{r} \phi_{s,y}^{(1)} = 0 \\ \phi_{i,y}^{(1)} = 0 \\ \rho(\tfrac{1}{2}\phi_{s,y}^{(1)^2} + c_s^{(0)}\,\phi_{s,x}^{(1)} + \eta_s^{(1)}) = \tfrac{1}{2}\phi_{i,y}^{(1)^2} + c_s^{(0)}\,\phi_{s,x}^{(1)} + \eta_i^{(1)}, \end{array} \right\} \quad \text{on } y = 1; \tag{19} \tag{20} \tag{21}$$

and

$$\phi_{i,y}^{(1)} = 0 \quad \text{on } y = 0. \tag{22}$$

The solution to the first-order problem is

$$\phi_{s,x}^{(1)} = -\frac{\eta_s^{(1)}}{c_s^{(0)}}, \tag{23}$$

$$\phi_{i,x}^{(1)} = \frac{-1}{c_i^{(0)}}[(1 - \rho)\,\eta_i^{(1)} + \rho\eta_s^{(1)}]. \tag{24}$$

In (23) and (24), $c_s^{(0)}$ and $c_i^{(0)}$ are the critical velocities of the upstream uniform flows and will be determined by the solvability condition of the second-order problem. The first-order elevations $\eta_s^{(1)}$ and $\eta_i^{(1)}$ will be determined by the solvability condition of the third-order problem.

The second-order problem:

$$\phi_{s,yy}^{(2)} = -\phi_{s,xx}^{(1)}, \tag{25}$$

$$\phi_{i,yy}^{(2)} = -\phi_{i,xx}^{(1)}, \tag{26}$$

$$\left. \begin{array}{r} \phi_{2,y}^{(2)} = c_s^{(0)}\,\eta_{s,x}^{(1)} \\ \phi_{s,t}^{(1)} + \tfrac{1}{2}\phi_{s,x}^{(1)^2} + c_s^{(0)}\,\phi_{s,x}^{(2)} + \lambda_s\,\phi_{s,x}^{(1)} + \eta_s^{(2)} + \rho^{-1}\bar{p} = 0, \end{array} \right\} \quad \text{on } y = 1 + \sigma, \tag{27} \tag{28}$$

$$\left. \begin{array}{r} \phi_{s,y}^{(2)} = c_s^{(0)}\,\eta_{i,x}^{(1)}, \\ \phi_{i,y}^{(2)} = c_i^{(0)}\,\eta_{i,x}^{(1)}, \\ \rho[\phi_{s,t}^{(1)} + \tfrac{1}{2}\phi_{s,x}^{(1)^2} + c_s^{(0)}\,\phi_{s,x}^{(2)} + \lambda_s\,\phi_{s,x}^{(1)} + \eta_i^{(2)}] \\ = \phi_{i,t}^{(1)} + \tfrac{1}{2}\phi_{i,x}^{(1)^2} + c_i^{(0)}\,\phi_{i,x}^{(2)} + \lambda_i\,\phi_{i,x}^{(1)} + \eta_i^{(2)}, \end{array} \right\} \quad \text{on } y = 1, \tag{29} \tag{30} \tag{31}$$
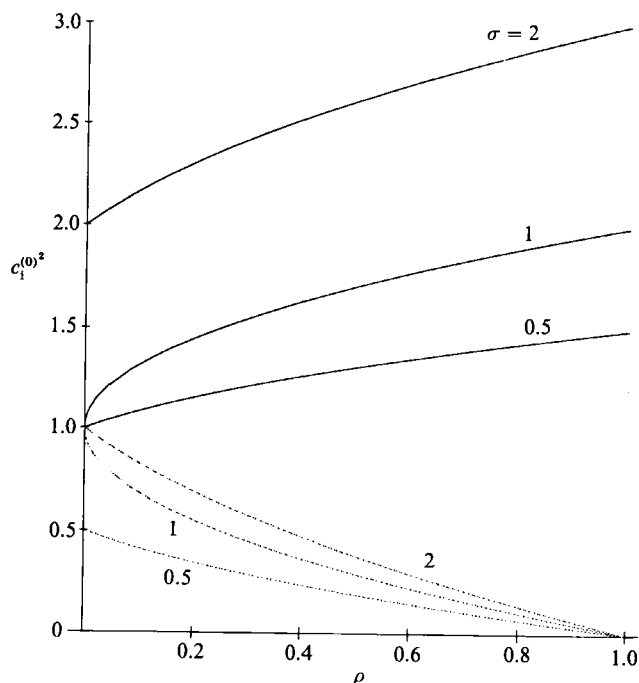
FIGURE 2. The dependence of the upstream critical velocity of the internal layer on the density ratio of the two fluids for $\gamma = 1$ and $\sigma = 0.5, 1, 2$. The solid lines are for the fast mode and the dotted lines for the slow mode.

and
$$\phi_{i,y}^{(2)} = 0 \quad \text{on } y = 0. \tag{32}$$

Using (25), (27) and (29), one can derive that
$$(c_s^{(0)^2} - \sigma)\,\eta_{s,x}^{(1)} - c_s^{(0)^2}\,\eta_{i,x}^{(1)} = 0. \tag{33}$$

Using (26), (32) and (30), one can similarly derive that
$$-\rho\eta_{s,x}^{(1)} + (c_i^{(0)^2} - 1 + \rho)\,\eta_{i,x}^{(1)} = 0. \tag{34}$$

The solvability condition of (33) and (34) for non-trivial solutions $(\eta_{s,x}^{(1)}, \eta_{i,x}^{(1)})$ is that the determinant of the coefficient matrix vanishes, i.e.
$$(c_s^{(0)^2} - \sigma)(c_i^{(0)^2} - 1) = \rho\sigma. \tag{35}$$

This is called the dispersion relation which determines the critical velocities $c_s^{(0)}$ and $c_i^{(0)}$. However (35) is underdetermined unless we specify the ratio of the upstream uniform velocity of the surface layer to that of the internal layer, γ:
$$\gamma = c_s^* / c_i^*. \tag{36}$$
By (1), we have
$$c_s^{(0)} = \gamma c_i^{(0)}, \quad \lambda_s = \gamma\lambda_i. \tag{37}$$

From (35), the critical velocities are given by
$$c_i^{(0)^2} = \frac{1}{2\gamma^2}[(\gamma^2 + \sigma) \pm ((\gamma^2 - \sigma)^2 + 4\gamma^2\sigma\rho)^{\frac{1}{2}}]. \tag{38}$$

The ' $+$ ' and ' $-$ ' correspond to the fast mode and slow mode of the upstream flow, respectively. This result agrees with equation (3.4) of Peters & Stoker (1960) when $\gamma = 1$. See figure 2 for the above relation. Even for the slow mode, the right-hand side is still greater than zero as long as $\rho \leqslant 1$. Hence the complex-valued upstream velocity corresponds to the Helmholtz instability.

For the single-layer flow with depth one, one has $\sigma = 0$, so $c_i^{(0)} = 1$ for the fast mode. This value one is the well-known critical Froude number. The slow mode for the single-layer flow is rest water.

For a single-layer flow of depth 2, one has $\sigma = 1$, $\rho = 1$. Then for the fast mode $c_i^{(0)^2} = (\gamma^2 + 1)/\gamma^2$. If the velocity ratio $\gamma = 1$, then $c_i^{(0)^2} = 2$. Here the total depth of the upstream fluid is $H = 2H_i$, and the critical Froude number is $(gH)^{\frac{1}{2}} = \sqrt{2}(gH_i)^{\frac{1}{2}}$, which is equal to $c_i^{(0)}(gH_i)^{\frac{1}{2}}$ in terms of the notations for two-layer flows in this paper. Hence $c_i^{(0)^2} = 2$ and this result agrees with the above result for a single-layer flow of depth one.

Next we integrate (25) and (26) with respect to y and with consideration of the boundary conditions. Finally the Bernoulli equations (28) and (31) yield the following expressions for $\phi_s^{(2)}$ and $\phi_i^{(2)}$ in terms of lower-order parameters:

$$\phi_{s,xx}^{(2)} = -\frac{1}{c_s^{(0)}}[\phi_{s,xt}^{(1)} + \lambda_s \phi_{s,xx}^{(1)}] \quad \text{(wave propagation term)}$$

$$-\frac{1}{c_s^{(0)}}\phi_{s,x}^{(1)}\phi_{s,xx}^{(1)} \quad \text{(nonlinear term)}$$

$$+[-\tfrac{1}{2}y^2 - (c_s^{(0)^2} - 1 - \sigma)y + \tfrac{1}{2}(1+\sigma)^2 + (c_s^{(0)^2} - 1 - \sigma)(1+\sigma)]\phi_{s,xxxx}^{(1)}$$
$$\text{(dispersion term)}$$

$$-\frac{1}{\rho c_s^{(0)}}\bar{p}_{,x} \quad \text{(forcing term)}$$

$$-\frac{1}{c_s^{(0)}}\eta_{s,x}^{(2)} \quad \text{(for the solvability of the third-order problem)}, \qquad (39)$$

$$\phi_{i,xx}^{(2)} = -\frac{1}{c_s^{(0)}}(c_s^{(0)^2} - \sigma)(\phi_{i,xt}^{(1)} + \lambda_i \phi_{i,xx}^{(1)}) \quad \text{(wave propagation term)}$$

$$-\frac{c_i^{(0)}}{c_s^{(0)^2}}(c_s^{(0)^2} - \sigma)^2 \phi_{i,x}^{(1)}\phi_{i,xx}^{(1)} \quad \text{(nonlinear term)}$$

$$+\left[\frac{c_i^{(0)}}{c_s^{(0)}}(c_s^{(0)^2} - \sigma)(-\tfrac{1}{2}y^2 + \tfrac{1}{2}) + \sigma\rho(c_s^{(0)^2} - \tfrac{1}{2}\sigma)\right]\phi_{s,xxxx}^{(1)} \quad \text{(dispersion term)}$$

$$-\frac{\bar{p}_{,x}}{c_i^{(0)}} \quad \text{(forcing term)}$$

$$+\frac{1}{c_i^{(0)}}[(\rho-1)\eta_{i,x}^{(2)} - \rho\eta_{s,x}^{(2)}] \quad \text{(for the solvability of the}$$

$$\text{third-order problem}). \qquad (40)$$

Here $\phi_s^{(1)}$ and $\phi_i^{(1)}$ are determined by (23) and (24). The first-order elevations $\eta_s^{(1)}$ and $\eta_i^{(1)}$ are not yet determined. This will be done by the solvability condition of the problem of next order.

The third-order problem:

$$\phi_{s,yy}^{(3)} = -\phi_{s,xx}^{(2)}, \tag{41}$$

$$\phi_{i,yy}^{(3)} = -\phi_{i,xx}^{(2)}, \tag{42}$$

$$\eta_{s,t}^{(1)} + c_s^{(0)}\,\eta_{s,x}^{(2)} + \lambda_s\,\eta_{s,x}^{(1)} + \phi_{s,x}^{(1)}\,\eta_{s,x}^{(1)} = \phi_{s,y}^{(3)} + \phi_{s,yy}^{(2)}\,\eta_s^{(1)} \quad \text{on } y = 1 + \sigma; \tag{43}$$

$$\eta_{i,t}^{(1)} + c_s^{(0)}\,\eta_{i,x}^{(2)} + \lambda_s\,\eta_{i,x}^{(1)} + \phi_{s,x}^{(1)}\,\eta_{i,x}^{(1)} = \phi_{s,y}^{(3)} + \phi_{s,yy}^{(2)}\,\eta_i^{(1)}, \quad \left.\right\} \tag{44}$$

$$\eta_{i,t}^{(1)} + c_i^{(0)}\,\eta_{i,x}^{(2)} + \lambda_i\,\eta_{i,x}^{(1)} + \phi_{i,x}^{(1)}\,\eta_{i,x}^{(1)} = \phi_{i,y}^{(3)} + \phi_{i,yy}^{(2)}\,\eta_i^{(1)}, \quad \left.\right\} \text{ on } y = 1; \tag{45}$$

and

$$\phi_{i,y}^{(3)} = c_i^{(0)}\,h_{,x} \quad \text{on } y = 0. \tag{46}$$

Integration of (41) in $[1, 1+\sigma]$ and (42) in $[0,1]$ with respect to y, with the boundary conditions, results in the following:

$$(c_s^{(0)^2} - \sigma)\,\eta_{s,x}^{(2)} - c_s^{(0)^2}\,\eta_{i,x}^{(2)} = -\frac{2\sigma}{c_s^{(0)}}(\eta_{s,t}^{(1)} + \lambda_s\,\eta_{s,x}^{(1)}) + \frac{3\sigma}{c_s^{(0)^2}}\eta_s^{(1)}\,\eta_{s,x}^{(1)}$$

$$+\,\sigma^2\left(-\tfrac{1}{6}\sigma + \tfrac{1}{2}c_s^{(0)^2}\right)\eta_{s,xxx}^{(1)} + \frac{\sigma}{\rho}\bar{p}_{,x}, \tag{47}$$

$$-\rho\eta_{s,x}^{(2)} + (c_i^{(0)^2} - 1 + \rho)\,\eta_{i,x}^{(2)} = -2c_i^{(0)}\left(1 - \frac{\sigma}{c_s^{(0)^2}}\right)(\eta_{s,t}^{(1)} + \lambda_i\,\eta_{s,x}^{(1)}) + 3c_i^{(0)^2}\left(1 - \frac{\sigma}{c_s^{(0)^2}}\right)^2\eta_s^{(1)}\,\eta_{s,x}^{(1)}$$

$$+\left[\tfrac{1}{3}c_i^{(0)^2}\left(1 - \frac{\sigma}{c_s^{(0)^2}}\right) + \rho\sigma\frac{c_i^{(0)}}{c_s^{(0)}}(c_s^{(0)^2} - \tfrac{1}{2}\sigma)\right]\eta_{s,xxx}^{(1)} + \bar{p}_{,x} + c_i^{(0)^2}\,h_{,x}. \tag{48}$$

The determinant of the coefficient matrix of (47) and (48) vanishes because of the solvability condition of the second-order problem (see the dispersion relation (35)). The solvability condition of (47) and (48) for $\eta_{s,x}^{(2)}$ and $\eta_{i,x}^{(2)}$ is that the inhomogeneous part is perpendicular to the null space of the conjugate matrix of the coefficient matrix. This orthogonality condition leads to the forced Koteweg–de Vries equation (fKdV) we desired to obtain:

$$m_1\,\eta_{s,t}^{(1)} + m_2\,\eta_{s,x}^{(1)} + m_3\,\eta_s^{(1)}\,\eta_{s,x}^{(1)} + m_4\,\eta_{s,xxx}^{(1)} = \tfrac{1}{2}f_{,x}, \tag{49}$$

where the coefficients m_k, $k = 1, 2, 3, 4$ and $f(x)$ are

$$m_1 = \frac{1}{c_s^{(0)^2}}[\sigma\rho c_s^{(0)} + c_i^{(0)}(c_s^{(0)^2} - \sigma)^2], \tag{50}$$

$$m_2 = \frac{1}{c_s^{(0)^2}}[\sigma\rho c_s^{(0)}\lambda_s + c_i^{(0)}(c_s^{(0)^2} - \sigma)^2\lambda_i], \tag{51}$$

$$m_3 = -\frac{3}{2c_s^{(0)^2}}\left[\sigma\rho + \left(\frac{c_i^{(0)}}{c_s^{(0)}}\right)^2(c_s^{(0)^2} - \sigma)^3\right], \tag{52}$$

$$m_4 = -\tfrac{1}{6}\left[\tfrac{1}{2}\sigma^2\rho(3c_s^{(0)^2} - \sigma) + (c_s^{(0)^2} - \sigma)\left(\left(\frac{c_i^{(0)}}{c_s^{(0)}}\right)^2(c_s^{(0)^2} - \sigma) + 3\sigma\rho\frac{c_i^{(0)}}{c_s^{(0)}}(c_s^{(0)^2} - \tfrac{1}{2}\sigma)\right)\right], \tag{53}$$

$$f(x) = c_s^{(0)^2}\,\bar{p}(x) + c_i^{(0)^2}(c_s^{(0)^2} - \sigma)\,h(x). \tag{54}$$

The upstream condition of uniform flow implies that

$$\eta_s^{(1)}(-\infty) = \eta_{s,x}^{(1)}(-\infty) = \eta_{s,xx}^{(1)}(-\infty) = 0. \tag{55}$$

The fKdV (49) and the upstream boundary condition (55) determine the first-order free-surface elevation $\eta_s^{(1)}$. The first-order interface elevation $\eta_i^{(1)}$ is then determined by (33), i.e.

$$\eta_i^{(1)} = \left(1 - \frac{\sigma}{c_s^{(0)^2}}\right)\eta_s^{(1)}. \tag{56}$$

With specified γ, $c_s^{(0)^2} - \sigma > 0$ for the fast mode. Hence $\eta_i^{(1)}$ and $\eta_s^{(1)}$ are of the same sign (sometimes referred to as the same phase). In contrast, $c_s^{(0)^2} - \sigma < 0$ for the slow mode. Hence $\eta_i^{(1)}$ and $\eta_s^{(1)}$ are of opposite signs (opposite phases) for the slow mode.

For a single-layer flow of depth one, we have $\sigma = 0$, $c_s^{(0)} = c_i^{(0)} = 1$, $m_1 = 1$, $m_2 = \lambda_i$, $m_3 = -\frac{3}{2}$, $m_4 = -\frac{1}{6}$, and $f(x) = \bar{p}(x) + h(x)$. This is the same as the fKdV derived by Mei (1986).

For a single-layer flow of depth 2, we have $\sigma = 1$, $\rho = 1$, $\gamma = 1$, $c_s^{(0)} = c_i^{(0)} = \sqrt{2}$, $m_1 = \sqrt{2}$, $m_2 = \sqrt{2}\lambda_i$, $m_3 = -\frac{3}{2}$, $m_4 = -\frac{4}{3}$, and $f(x) = 2(\bar{p}(x) + h(x))$.

In general, for a single-layer flow of depth d, we have $\sigma = d - 1$, $\rho = 1$, $\gamma = 1$, $c_i^{(0)} = c_s^{(0)} = d^{\frac{1}{2}}$, $m_1 = d^{\frac{1}{2}}$, $m_2 = d^{\frac{1}{2}}\lambda_i$, $m_3 = -\frac{3}{2}$, $m_4 = -\frac{1}{6}d^3$, and $f(x) = d(\bar{p}(x) + h(x))$. This agrees with the fKdV derived by Shen (1989) for a rectangular channel and may be considered as a verification of the correctness of the coefficients (50)–(54).

3. Solitary waves and turning-point bifurcations

In this section we consider the stationary solitary wave solutions of the fKdV (49). Namely, we investigate all possible solutions of the following ordinary differential equation boundary-value problem:

$$m_2 \eta_s^{(1)} + \frac{1}{2}m_3 \eta_s^{(1)^2} + m_4 \eta_{s,xx}^{(1)} = \frac{1}{2}f(x), \tag{57}$$

$$\eta_s^{(1)}(\pm\infty) = \eta_{s,x}^{(1)}(\pm\infty) = 0. \tag{58}$$

The upstream velocity perturbation is included in the coefficient m_2. Hence it is m_2 that controls the solitary wave solutions of (57) and (58). m_2 is always positive when λ_i and λ_s are positive. By (35) one can show that when

$$\rho > \left(\frac{\sigma}{\gamma}\right)^2 \quad \text{and} \quad \frac{3\sigma^2(1-\gamma)}{2\gamma} < 1, \tag{59}$$

then $m_3 < 0$ and $m_4 < 0$, for any $0 \leqslant \rho \leqslant 1$ and non-negative γ (see figure 3). For some other values of σ, ρ and γ, m_3 and m_4 may be zero or positive. Then our asymptotically reduced equation above (the fKdV) becomes invalid because of the disappearance, or the adverse effect, of the nonlinearity and the dispersion. It implies that the second-order nonlinearity in the fKdV does not include a somewhat stronger nonlinearity intrinsic to the system. A higher-order nonlinearity must be included at the beginning of the asymptotic expansion. We will briefly discuss such a situation in §6. Here we concentrate on the case of second-order nonlinearity, which is warranted by (59).

With specified parameters γ, ρ and σ, we shall find the solutions of the boundary-value problem (57) and (58). The solutions will depend on the upstream velocity perturbation parameter λ_i. One can prove that when m_2 is sufficiently large, there exists at least one solution to the problem (57) and (58). This was proved by Shen (1989) by using the contraction mapping theorem. Further we have

THEOREM 1. *If $f(x) \geqslant 0$ and has compact support, and if (59) holds, then there exists $\lambda_C > 0$ such that the problem (57) and (58) has at least two positive solutions when $\lambda > \lambda_C$.*
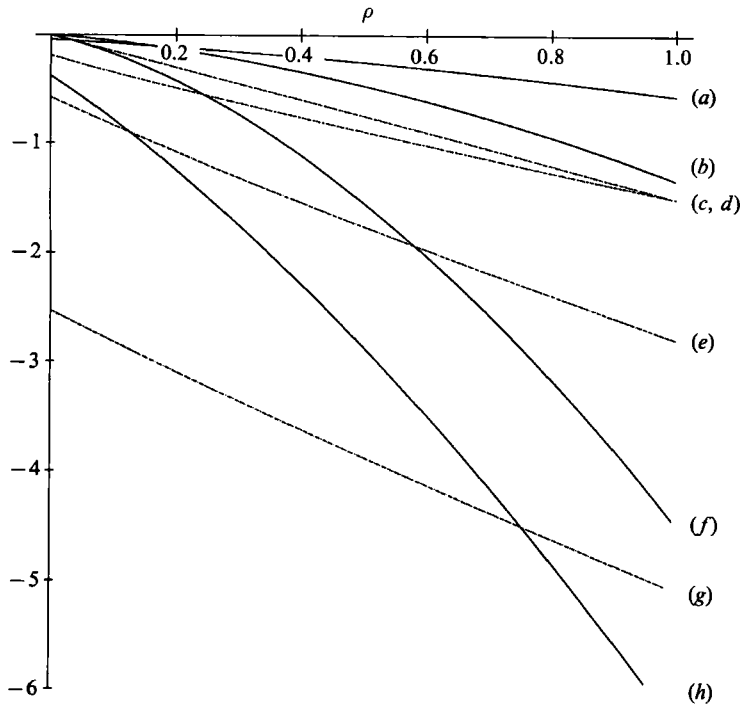
FIGURE 3. The dependence of m_3 and m_4 on σ, γ and ρ for the fast mode. Curve (a) $m_4, \sigma = 0.5$, $\gamma = 1$; (b) $m_4, \sigma = 1$, $\gamma = 1$; (c) $m_3, \sigma = 1$, $\gamma = 1$; (d) $m_3, \sigma = 0.5$, $\gamma = 1$; (e) $m_3, \sigma = 1$, $\gamma = 1.5$; (f) $m_4, \sigma = 2$, $\gamma = 1$; (g) $m_3, \sigma = 1$, $\gamma = 2$; and (h) $m_4, \sigma = 1$, $\gamma = 2$.

The proof of the theorem is the same as that for a similar theorem due to Shen (1989). In the case of local forcing, the value of λ_C can be analytically found. In turn, one can determine the upstream Froude number $U_C/(gH)^{\frac{1}{2}} = 1 + \epsilon \lambda_C$ for single-layer flows. This agrees with a formula first derived by Miles (1986) when ϵ is very small. See §5.2 for more details.

Let $u(x)$ and $v(x)$ be solutions of (57) and (58). Let a be the left-most local maximum point for both $u(x)$ and $v(x)$. If $u(a) = v(a)$, then $u(x) = v(x)$ for any x, for the solution to the problem

$$m_2 u + \tfrac{1}{2} m_3 u^2 + m_4 u'' = \tfrac{1}{2} f(x), \quad x > a;$$

$$u(a) = N > 0, \quad u'(a) = 0, \quad u(\infty) = u'(\infty) = 0$$

is unique.

Therefore the solutions to the problem (57) and (58) can be distinguished by the left-most local maximum values. Let $z = \inf\{x \mid x \in \Re$, where $u'(x) = 0$, u is a solution of (57) and (58)$\}$ and $N = u(z) > 0$. Then $u(x)$ is monotonically increasing in $(-\infty, z)$ and has an inverse

$$x = X(u; N), \quad u \in (0, N).$$

Multiplying (57) by $u'(x)$, where $u(x)$ is a solution of (57) and (58), and integrating the resulting equation with respect to x in $(-\infty, z)$, we have

$$m_2 = -\tfrac{1}{3} m_3 N + \frac{1}{N^2} \int_0^N f(X(u; N)) \, du. \tag{60}$$

Let $\lambda = \lambda_1$ and

$$\bar{m} = \frac{c_i^{(0)}}{c_s^{(0)^2}} [\sigma \rho \gamma^2 + (c_s^{(0)^2} - \sigma)^2] > 0. \tag{61}$$

Then

$$\lambda = m_2/\bar{m}. \tag{62}$$

Equations (60)–(62) define a curve Γ in the (λ, N)-plane. The curve Γ is called the bifurcation diagram. It has two straight line asymptotes,

$$N = -\frac{3\bar{m}\lambda}{m_3}, \quad N = 0. \tag{63}$$

If Γ is connected, then the structure of the asymptotes implies the existence of at least one turning point, i.e. λ_C. At this turning point, the vertical line $\lambda = \lambda_C$ is tangent to Γ at (λ_C, N_C). For positive forcing $f(x) \geqslant 0$, one has $\lambda_C > 0$ from the three bifurcation equations above.

For the locally forced case, $f(x) = 2P\delta(x)$. Both the Dirac delta function $\delta(x)$ and the solutions $u(x)$ are generalized functions. The usual product of two generalized functions is not defined. Hence the bifurcation equation (60) cannot be used any more. Fortunately, the solutions $u(x)$ and the bifurcation diagram Γ can be found analytically. When $f(x) = 2P\delta(x)$, all solutions to the ordinary differential equation boundary-value problem (57) and (58) can be written in the following form:

$$\eta_s^{(1)}(x) = -\frac{3m_2}{m_3}\operatorname{sech}^2\left(\frac{-m_2}{4m_4}\right)^{\frac{1}{2}}\begin{cases}(x - L_0) & \text{if } x \geqslant 0, \\ (x + L_0) & \text{if } x < 0,\end{cases}$$

where $$L_0 = (4m_4/{-m_2})^{\frac{1}{2}}\operatorname{arctanh}(b), \tag{64}$$

and b is in $(-1, 1)$ and satisfies the following third-order algebraic equation:

$$b^3 - b + \frac{m_3 P}{6m_2(-m_2 m_4)^{\frac{1}{2}}} = 0. \tag{65}$$

When $m_2 = m_C$,

$$m_C = \left(\frac{3m_3^2 P^2}{-16m_4}\right)^{\frac{1}{3}}, \tag{66}$$

(65) has a double root in $(-1, 1)$ and the third root is outside $(-1, 1)$. This is the point at which the two solitary waves associated with this mode merge into one. Hence the turning point $\lambda_C = m_C/\bar{m}$ is found to be

$$\lambda_C = \frac{1}{\bar{m}}\left(\frac{3m_3^2 P^2}{-16m_4}\right)^{\frac{1}{3}}.$$

For positive local forcings, $P > 0$, the bifurcation diagram is analytically given below

$$\|\eta_s^{(1)}\|_\infty = -\tfrac{1}{4}P\left(\frac{-3}{m_2 m_4}\right)^{\frac{1}{2}}\left(\cos\left[\tfrac{1}{3}\arccos\left(\frac{-\sqrt{3}Pm_3}{4(-m_4 m_2^3)^{\frac{1}{2}}}\right) + \left\{\begin{matrix}\tfrac{4}{3}\pi\\\tfrac{2}{3}\pi\end{matrix}\right\}\right]\right)^{-1}. \tag{67}$$

The $(\|\eta_s^{(1)}\|_\infty, \lambda)$-curve defined above has two branches: the upper and lower branches correspond to $\tfrac{4}{3}\pi$ and $\tfrac{2}{3}\pi$ respectively. The two branches are joined at the turning point λ_C, at which $\|\eta_s^{(1)}\|_\infty = -2m_C/m_3$. As $\lambda \to \infty$, the $(\|\eta_s^{(1)}\|_\infty, \lambda)$-curve has two asymptotes: $-3\bar{m}\lambda/m_3$ for the upper branch and $P/[2(-m_4\bar{m}\lambda)^{\frac{1}{2}}]$ for the lower branch. Therefore, the asymptote for the upper branch solutions is a straight line and that for the lower branch is a parabola, and the λ-axis is in turn the straight line asymptote of the parabola. Figure 5 below shows these geometric results.

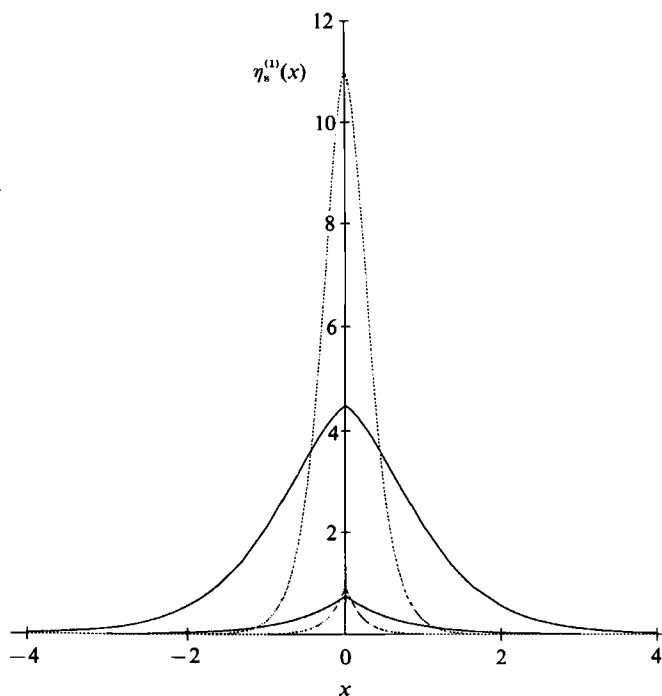For $\sigma = 1$, $\gamma = 1$, $\rho = 0.5$, $P = 1$, the four solutions are shown in figure 4 when

FIGURE 4. Four supercritical solitary wave solutions of the locally forced fKdV problem (57) and (58) when $\sigma = 1$, $\gamma = 1$, $\rho = 0.5$ and $P = 1$. The solid curves correspond to the fast mode and the dotted curves to the slow mode.

$\lambda = 1.5$. The bifurcation diagrams are shown in figure 5 for $P = 2, 1$. These figures were very easily generated by the symbolic computer routine Mathematica.

Now let us look at the case of non-local forcing. To solve the problem (57) and (58) one has to use a numerical method. The difficulty in finding numerical solutions of (57) and (58) is in distinguishing one solution from the other with the same equation and the same boundary data at $-\infty$ and ∞. Shen (1989) found an efficient and reliable numerical scheme to find multiple solutions of (57) and (58). We recapitulate it below. Let $f \in C_0^\infty(\Re)$, $x_- = \inf \mathrm{supp}\,(f)$, $x_+ = \sup \mathrm{supp}\,(f)$. The analytical solution of the problem (57) and (58) from $-\infty$ to x_- is

$$\eta_s^{(1)}(x) = -\frac{3m_2}{m_3} \mathrm{sech}^2 \left(\frac{-m_2}{4m_4}\right)^{\frac{1}{2}} (x - L_0), \quad x \leqslant x_-.$$

Different solutions are distinguished by different values of the phase shift L_0. To determine this phase shift L_0, we introduce a new quantity B as follows:

$$B(x, \lambda, L_0) = \int_{x_-}^x \tfrac{1}{2} f(\xi)\, \eta_{s,x}^{(1)}(\xi)\, d\xi$$

$$= \tfrac{1}{2} m_4 (\eta_{s,x}^{(1)}(x))^2 + (\tfrac{1}{2} m_2 + \tfrac{1}{6} m_3\, \eta_s^{(1)}(x))\, (\eta_s^{(1)}(x))^2.$$

It is clear that $B(x, \lambda, L_0) = B(x_+, \lambda, L_0)$ for every $x \geqslant x_+$. One can show (Benjamin & Lighthill 1954) that $\eta_s^{(1)}(\infty) = \eta_{s,x}^{(1)}(\infty) = 0$ if and only if

$$B(x_+, \lambda, L_0) = 0 \quad \text{and} \quad 0 \leqslant \eta_s^{(1)}(x_+) < -3m_2/m_3.$$
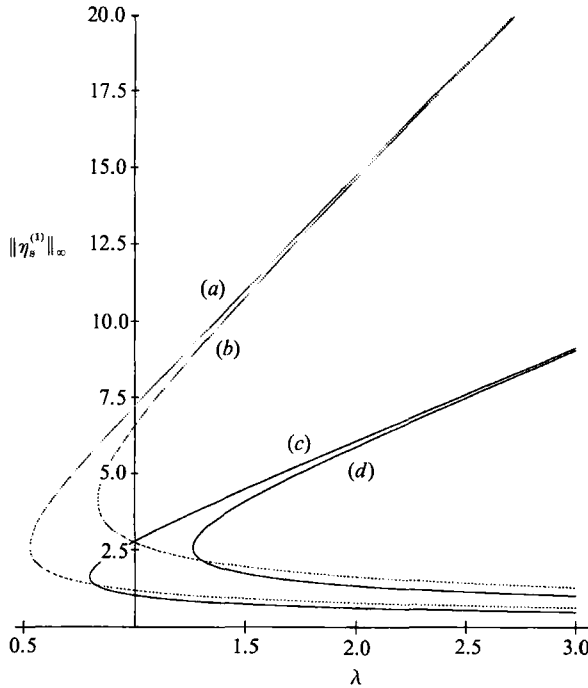
This condition determines the phase shift L_0.

FIGURE 5. The turning point bifurcation diagram of the locally forced fKdV problem (57) and (58) when $\sigma = 1, \gamma = 1$, and $\rho = 0.5$. The solid curves correspond to the fast mode and the dotted curves to the slow mode. Curve (a) $P = 1$, slow mode; (b) $P = 2$, slow mode; (c) $P = 1$, fast mode; and (d) $P = 2$, fast mode.

Therefore we solve the following initial-value problem:

$$m_2\,\eta_s^{(1)} + \tfrac{1}{2}m_3\,\eta_s^{(1)^2} + m_4\,\eta_{s,\,xx}^{(1)} = \tfrac{1}{2}f(x), \quad x > x_-,$$

$$\eta_s^{(1)}(x_-) = -\frac{3m_2}{m_3}\operatorname{sech}^2\left(\frac{-m_2}{4m_4}\right)^{\frac{1}{2}}(x_- - L_0),$$

$$\eta_{s,\,x}^{(1)}(x_-) = -\left(-\frac{m_2}{m_4}\right)^{\frac{1}{2}}\eta_s^{(1)}(x_-)\tanh\left(\frac{-m_2}{4m_4}\right)^{\frac{1}{2}}(x_- - L_0)$$

up to x_+ for a given L_0. $B(x_+, \lambda, L_0)$ can be computed. Repeating the above process by a do-loop for L_0, we obtain an (L_0, B)-curve. The intersections of this curve with the L_0-axis are the solutions of $B(x_+, \lambda, L_0) = 0$ for prescribed x_+ and λ. Therefore the number of solitary wave solutions to the fKdV equals the number of zeros of $B(x_+, \lambda, L_0)$.

The above scheme was implemented by a Mathematica package called NumericalMath/RungeKutta.m on the SUN SPARCstation $1+$. As an example, we let $\sigma = 1$, $\rho = 0.5$, $\gamma = 1$, $\lambda = 1.2$ and

$$f(x) = \begin{cases} 2(1 - x^2)^{\frac{1}{2}} & \text{if } |x| \leqslant 1, \\ 0 & \text{elsewhere.} \end{cases}$$

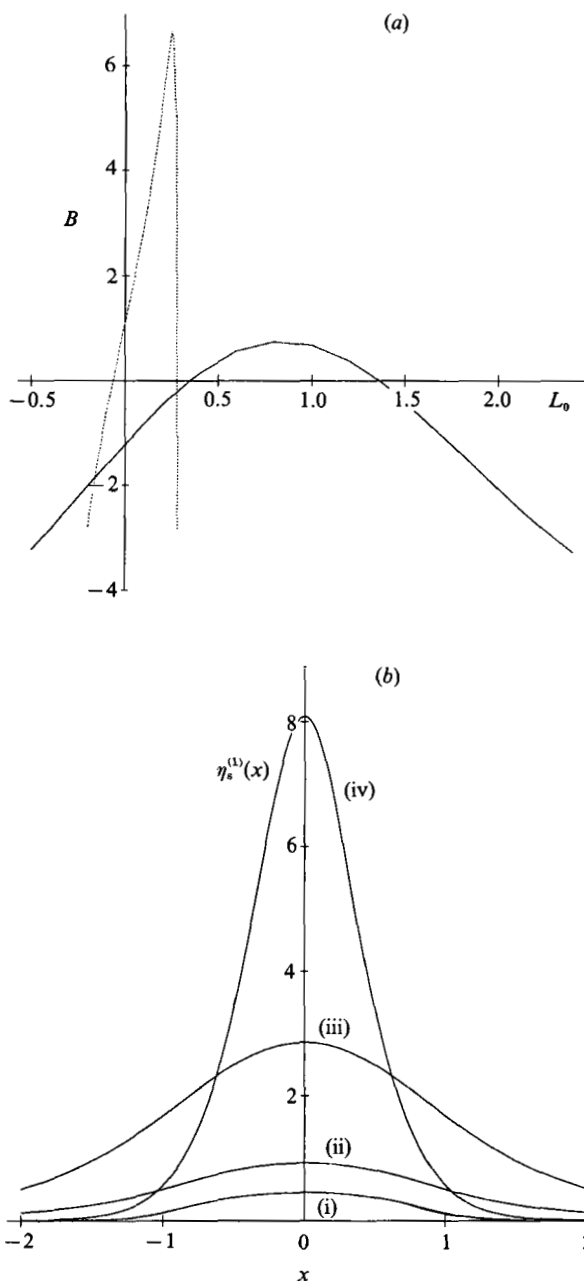The corresponding (B, L_0)-curve and the solutions to (57) and (58) are shown in figures 6(a) and 6(b) respectively.

FIGURE 6. (a) The B, L_0 relationship when $\sigma = 1$, $\gamma = 1$, $\rho = 0.5$, $\lambda = 1.2$ and when the non-local forcing is

$$f(x) = \begin{cases} 2(1-x^2)^{\frac{1}{2}} & \text{if} \quad |x| \leqslant 1, \\ 0 & \text{elsewhere.} \end{cases}$$

The solid curves correspond to the fast mode and the dotted curves to the slow mode. (b) The four supercritical solitary wave solutions correspond to the data in part (a). The phase shift for each of the solutions is: curve (i) $\Leftrightarrow L_0 = 0.278065$, (ii) $\Leftrightarrow L_0 = 1.360600$, (iii) $\Leftrightarrow L_0 = 0.347700$, (iv) $\Leftrightarrow L_0 = -0.065743$. Solutions (i) and (iv) are for the slow mode, and solutions (ii) and (iii) the fast mode.
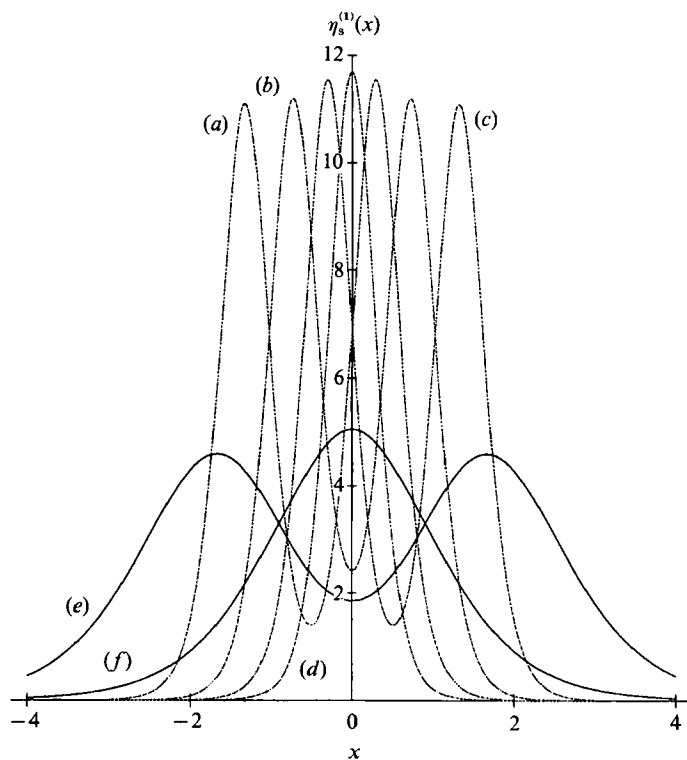
FIGURE 7. Six supercritical solutions of the fKdV problem (57) and (58) for non-local negative forcing

$$f(x) = \begin{cases} -2(1-x^2)^{\frac{1}{2}} & \text{if} \quad |x| \leqslant 1, \\ 0 & \text{elsewhere,} \end{cases}$$

and $\sigma = 1$, $\gamma = 1$, $\rho = 0.5$, $\lambda = 1.5$. The solid lines correspond to the fast mode: $m_1 = 0.7654$, $\bar{m} = 0.7654$, $m_3 = -0.75$, $m_4 = -0.4684$. The dotted lines correspond to the slow mode: $m_1 = 1.8478$, $\bar{m} = 1.8478$, $m_3 = -0.75$, $m_4 = -0.1149$. The phase shifts are: curve $(a) \Leftrightarrow L_0 = -1.324417$, $(b) \Leftrightarrow L_0 = -0.731526$, $(c) \Leftrightarrow L_0 = -0.284012$, $(d) \Leftrightarrow L_0 = 0.082742$, $(e) \Leftrightarrow L_0 = -1.666355$ and $(f) \Leftrightarrow L_0 = -0.146660$.

For some non-local negative forcings, surprisingly there can exist more than four solitary wave solutions to (57) and (58). For the negative semi-elliptical forcing

$$f(x) = \begin{cases} -2(1-x^2)^{\frac{1}{2}} & \text{if} \quad |x| \leqslant 1, \\ 0 & \text{elsewhere} \end{cases}$$

and $\lambda = 1.5$, there are six solitary wave solutions. Two of them correspond to the fast mode and the other four correspond to the slow mode. Among the four solutions for the slow mode, two of them are non-symmetric with respect to the origin even though the forcing is symmetric. See figure 7 for the six solutions.

One can naturally make a guess that there may exist eight solitary wave solutions, four for the slow mode and four for the fast mode for some λ and some $f(x)$. This is indeed true. For the negative forcing in the above example, there are eight solutions when $\lambda = 5$. Whether there exist more than eight solutions for certain non-local negative forcing is yet to be investigated. Probably, the answer is yes.

4. Hydraulic falls

In this section we consider all the stationary solutions of the fKdV (49) when $m_2 < 0$. What is to be investigated is the following ordinary differential equation initial-value problem:

$$m_2 \eta_s^{(1)} + \tfrac{1}{2} m_3 \eta_s^{(1)^2} + m_4 \eta_{s, xx}^{(1)} = \tfrac{1}{2} f(x), \quad m_2 < 0, \quad x_- < x < \infty, \tag{68}$$

$$\eta_s^{(1)}(x_-) = \eta_{s, x}^{(1)}(x_-) = 0, \quad \text{and } \eta_s^{(1)} \text{ is bounded.} \tag{69}$$

We still assume (59) holds. This assumption ensures the formal validity of the model equation (68). In addition, we also keep the assumption that $f(x)$ is of compact base, i.e. $f(x) \equiv 0$ when $x \notin [x_-, x_+]$ for some real numbers x_- and x_+. It can be proved that, when $\lambda(= \lambda_1)$ is sufficiently small (negative), the initial-value problem (68) and (69) has a unique solution (Shen & Shen 1990).

The energy integration of the initial-value problem (68) and (69) in $[x_+, \infty)$ leads to a new initial-value problem of reduced order:

$$\frac{3m_4}{m_3} (\eta_{s, x}^{(1)})^2 = -\eta_s^{(1)^3} - \frac{3m_2}{m_3} \eta_s^{(1)^2} + D, \quad x > x_+, \tag{70}$$

$$\eta_s^{(1)} |_{x = x_+} = \eta_s^{(1)}(x_+). \tag{71}$$

Here

$$D = (\eta_s^{(1)}(x_+))^3 + \frac{3m_2}{m_3} (\eta_s^{(1)}(x_+))^2 + \frac{3m_4}{m_3} (\eta_{s, x}^{(1)}(x_+))^2. \tag{72}$$

The data $\eta_s^{(1)}(x_+)$ and $\eta_{s, x}^{(1)}(x_+)$ are obtained from the numerical integration of the initial-value problem (68) and (69) from x_- to x_+. Hence for a given forcing $f(x)$, $D = D(\lambda)$ is a function of only λ. Depending on the choice of the value of λ, the third-order algebraic equation

$$z^3 + \frac{3m_2}{m_3} z^2 - D = 0 \tag{73}$$

has three distinct real zeros, a double zero, or only one real zero. Correspondingly, the new initial-value problem (70) and (71) has a cnoidal wave (Stokes wave) solution, a hydraulic fall solution, or an unbounded solution respectively. The unbounded solution has no physical meaning and is outside the scope of our consideration.

When $f(x) \geqslant 0$, one can show that $D(\lambda) > 0$ and $D(\lambda)$ is bounded as $\lambda \to \infty$. Hence the equation

$$4\bar{m}^3 \lambda^3 / m_3^3 = D(\lambda) \tag{74}$$

has at least one solution λ_L. At this λ_L, (73) attains its real double root and the cnoidal wave solution approaches the hydraulic fall. Beyond this limit, the initial-value problem (70) and (71) does not have bounded solutions.

When (73) attains its double root, (70) and (71) can be integrated by an integration method in elementary calculus. The result is

$$\eta_s^{(1)} = \frac{2\bar{m}\lambda_L}{m_3} \left(-1 + \tfrac{3}{2} \operatorname{sech}^2 \left(\frac{\bar{m}\lambda_L}{4m_4} \right)^{\frac{1}{2}} (x - x_0) \right). \tag{75}$$

The phase shift x_0 is given by

$$x_0 = x_+ + 2 \left(\frac{m_4}{\bar{m}\lambda_L} \right)^{\frac{1}{2}} \operatorname{arcsech} \left(\frac{m_3 \eta_s^{(1)}(x_+) + 2\bar{m}\lambda_L}{3\bar{m}\lambda_L} \right)^{\frac{1}{2}}. \tag{76}$$

The free surface falls from $\eta_s^{(1)} = 0$ upstream to $\eta_s^{(1)} = -2\bar{m}\lambda_L/m_3$ downstream on the site of the forcing. This fall does not suffer any energy loss, and hence is different from the hydraulic jump described in fluid dynamics textbooks (see, for example, Yih 1979).

For the locally forced case, $f(x) = 2P\delta(x)$, one can derive the following:

$$\lambda_L = \frac{1}{\bar{m}}\left(\frac{3m_3^2 P^2}{4m_4}\right)^{\frac{1}{3}} < 0, \tag{77}$$

$$x_0 = 2(m_4/(\bar{m}\lambda_L))^{\frac{1}{2}}\,\text{arcsech}\,(\tfrac{2}{3})^{\frac{1}{2}}, \tag{78}$$

$$\eta_s^{(1)}(x) = \frac{2\bar{m}\lambda_L}{m_3}\left\{-1 + \tfrac{3}{2}\,\text{sech}^2\left(\frac{\bar{m}\lambda_L}{4m_4}\right)^{\frac{1}{2}}[x - 2(m_4/(\bar{m}\lambda_L))^{\frac{1}{2}}\,\text{arcsech}\,(\tfrac{2}{3})^{\frac{1}{2}}]\right\}. \tag{79}$$

In (79), when $x \to \infty$, one obtains the dimensionless amplitude of the hydraulic fall

$$\eta_s^{(1)}(\infty) = \left(\frac{6P^2}{m_3 m_4}\right)^{\frac{1}{3}}. \tag{80}$$

Therefore, the fall's amplitude is proportional to the strength of the forcing and inversely proportional to the strength of the nonlinearity and that of the dispersion.

In the next section, some examples of hydraulic fall will be seen and these examples are used to illustrate the comparison among the asymptotic, computational and experimental results.

5. Comparison of asymptotic, experimental and computational results

5.1. *Introduction to the comparison*

To compare the results obtained from asymptotic, computational and experimental methods, we need to convert all scales into the laboratory scales. The comparison can then be done under these calibrated scales. For the asymptotic approach, the basic concern is the shrinking of the horizontal lengthscale because of the long-wave assumption. For the direct numerical integration approach (i.e. the computational method), all the published literature takes the horizontal lengthscale to be the same as the vertical one.

Recalling the non-dimensionalization at the beginning of §2, one can convert the dimensionless fKdV (49) into the laboratory fKdV

$$m_1\,\eta_{s,\,t^*}^* + \bar{m}u_\lambda^*\,\eta_{s,\,x^*}^* + m_3\left(\frac{g}{H_i}\right)^{\frac{1}{2}}\eta_s^*\,\eta_{s,\,x^*}^* + m_4(gH_i)^{\frac{1}{2}}H_i^2\,\eta_{s,\,x^*x^*x^*}^*$$

$$= (gH_i)^{\frac{1}{2}}\left[\frac{c_s^{(0)^2}}{\rho_i g}\bar{p}_{x^*}^* + c_i^{(0)^2}(c_s^{(0)^2} - \sigma)\,h_{,x^*}^*\right]. \tag{81}$$

Here

$$u_\lambda^* = \epsilon\lambda_i(gH_i)^{\frac{1}{2}} \tag{82}$$

is the perturbation of the upstream velocity from the critical value.

Since there are no experimental and computational results simultaneously available for non-locally forced cases, we only consider the comparison in the case of local forcing. For this local forcing, there are two important parameters, ϵ and P, which are crucial to the response of the free boundaries. These two free boundaries
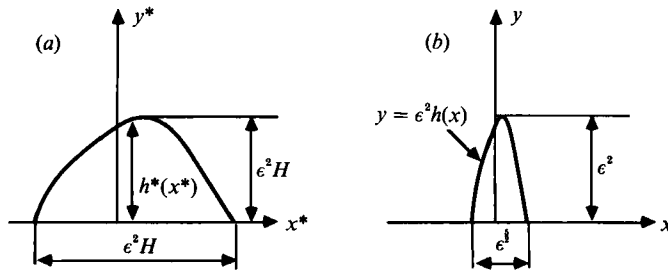
FIGURE 8. Shrinking of the base of the bump after the non-dimensionalization: (a) a bump in the laboratory, (b) the same bump in the fKdV scale.
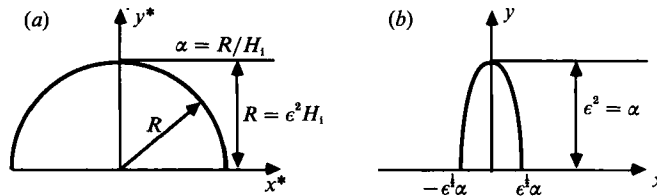

FIGURE 9. The same as figure 8 with specified bump shape: a semicircle in the laboratory.

are described by the functions $\eta_s^{(*)}(x^*, t^*)$ and $\eta_i^{(*)}(x^*, t^*)$ respectively. One should imagine that the value of ϵ should be determined by the nature of the physical assumptions. In this paper, the nature of the physical assumption in setting-up the experimental apparatus is reflected in that the forcing is of order ϵ^2. It is this assumption which leads to the determination of ϵ. However, this determination is not unique. Namely, the dimensionless 'small' quantity ϵ can take different values. The physical reason is that the physics should not depend on the choice of the small dimensionless parameter ϵ as long as the choice of ϵ is consistent with the physics. Mathematically, as soon as ϵ is chosen, the dimensionless forcing amplitude P should be determined accordingly. It turns out that the physical quantities depending on both ϵ and P take the same value for different values of ϵ. This is referred to as the ϵ-invariant property. That is, even though the quantity ϵ takes different values for the same problem, the physical quantities (like the maxima of solitary wave elevations, the amplitudes of hydraulic falls, etc.) computed from the fKdV theory are still the same. The details about the choice of ϵ and P as well as the ϵ-invariant property will be discussed in the next subsection.

5.2. The choice of the values of ϵ

Let the bump $y^* = H^*(x^*)$ be the only forcing (see figure 8a). In terms of the dimensionless asymptotic variables, the bump is $y = h(\epsilon^{-\frac{1}{2}}x)$ (denoted by $y = \epsilon^2 h(x)$ in §2) as shown in figure 8b). Let us concentrate on the case when the horizontal laboratory scale of the bump base is the same as the vertical one of the bump height. As an example, let us look at the semicircular bump: $y^* = (R^2 - x^{*2})^{\frac{1}{2}}$. In dimensionless asymptotic scales, $x = \epsilon^{\frac{1}{2}}x^*/H, y = y^*/H$, and the semicircular bump becomes $y = (1/\epsilon^{\frac{1}{2}})(\epsilon\alpha^2 - x^2)^{\frac{1}{2}}$ (see figure 9a, b). Here $\alpha = R/H$. The support of the bump is now $[-\epsilon^{\frac{1}{2}}\alpha, \epsilon^{\frac{1}{2}}\alpha]$, which is $\epsilon^{\frac{1}{2}}$ times smaller than the height α. This height α can be regarded as the amplitude of the forcing. Hence, $\epsilon^2 = \alpha$ by the assumption on the magnitude of the forcing in §2. Consequently,

$$\epsilon = \alpha^{\frac{1}{2}}. \tag{83}$$

Because of the short support in the dimensionless variable x in the asymptotic analysis, the bump is approximated by $Q\delta(x)$ in the dimensionless fKdV. Hence, $P = \frac{1}{2}Q$ for the forcing term $f(x) = 2P\delta(x)$ in the fKdV in §§3 and 4. The forcing amplitude will be determined by the area A under the semicircle, namely

$$\int_{-\infty}^{\infty} H^*(x^*)\,\mathrm{d}x^* = \int_{-\infty}^{\infty} \epsilon^2 H Q \delta(x)\,\mathrm{d}(\epsilon^{-\frac{1}{2}}Hx) = A.$$

This leads to

$$Q = \epsilon^{-\frac{3}{2}}A/H^2 \quad \text{or} \quad Q = (\tfrac{1}{2}\pi)\,\alpha^{\frac{3}{2}}. \tag{84}$$

Equations (83) and (84) determine the values of ϵ and Q for a given circular bump. For example, if $R = 0.25H$ (a quarter of the total depth for the single-layer flow), then $\alpha = 0.25$, $\epsilon = (0.25)^{\frac{1}{2}} = 0.5$, $Q = (\tfrac{1}{2}\pi)\,0.25^{\frac{3}{2}} = 0.1693$.

However, the choice of the ϵ value is not unique. What has been shown above is only one method to determine ϵ. When the area of the bump is known but not the exact shape, the above method is not valid and the following more general procedure can be used. It is still assumed that the height and base of the bump are of comparable length. Then, in the laboratory, the bump area can be measured in the scale H. Approximately, $\epsilon^2 H \times \epsilon^2 H = A$. This leads to

$$\epsilon = (A/H^2)^{\frac{1}{4}}. \tag{85}$$

The delta forcing amplitude Q is still given by $Q = \epsilon^{-\frac{3}{2}}A/H^2$. As an example, let $A = 0.0982H^2$. Then $\epsilon = 0.5598$, and $Q = 0.2345$.

In the case of semicircular bump forcing, $\alpha = R/H$, $\epsilon = ((\tfrac{1}{2}\pi)\,\alpha^2)^{\frac{1}{4}}$, and $Q = \pi^{-\frac{3}{8}}\alpha^{\frac{5}{4}}$. The above example then has $\alpha = 0.25$, which is the same as the earlier example. Now $\epsilon = 0.5598$, and $Q = 0.2345$. Obviously, this is a different choice of ϵ and Q from that given by (83) and (84), although we are considering the same bump. It remains to be shown that the different choices of ϵ and Q still yield the same free-surface elevation and all other physical quantities in the laboratory coordinates. This is a more detailed interpretation of what we referred to earlier as the ϵ-invariant property of the fKdV theory.

We have already seen from (81) that the free-surface elevation is ϵ-invariant since (81) is independent of ϵ. However, it is not obvious that the ϵ-invariant property does not change under the Dirac delta function approximation of the forcing. Nonetheless, we can show that indeed the ϵ-invariant property continues to hold under the Dirac delta function approximation. As an example, we consider only physical quantities U_C and U_L, which are upstream velocities corresponding to the turning point and cutoff point, respectively. We show that

THEOREM 2. *Under the Dirac delta function approximation, U_C and U_L are still ϵ-invariant in the fKdV theory for flows over a semicircular bump.*

Proof. $U_C = (gH)^{\frac{1}{2}}(c_0 + \epsilon\lambda_C)$, $U_L = (gH)^{\frac{1}{2}}(c_0 + \epsilon\lambda_L)$ recover the laboratory turning point velocity and cutoff velocity, respectively, from the asymptotic procedure. Namely, U_C and U_L are observable physical quantities in the laboratory. By the formulae for λ_C and λ_L derived in §§3 and 4, we have

$$U_C = (gH)^{\frac{1}{2}}\{1 + \epsilon P^{\frac{2}{3}}(1/\bar{m})[3m_3^2/(-16m_4)]^{\frac{1}{3}}\}, \tag{86}$$

$$U_L = (gH)^{\frac{1}{2}}\{1 + \epsilon P^{\frac{2}{3}}(1/\bar{m})[3m_3^2/(-4m_4)]^{\frac{1}{3}}\}. \tag{87}$$

The values of the dimensionless quantities $\bar{m}$, m_3 and m_4 have already been determined by the density ratio ρ, the velocity ratio γ and the depth ratio σ, and $\bar{m}$,

m_3 and m_4 are independent of ϵ. Hence, U_C and U_L are functions of ϵ and P according to (86) and (87), $U_C = U_C(\epsilon, P), U_L = U_L(\epsilon, P)$. So it is to be shown that $\epsilon P^{\frac{3}{2}}(\epsilon)$ does not change for different choices of ϵ.

As described a little earlier, $P = \frac{1}{2}Q$. When substituting $\epsilon = \alpha^{\frac{1}{2}}$ and $Q = \epsilon^{-\frac{3}{2}}A/H^2$ into $\epsilon P^{\frac{3}{2}}$, we obtain

$$\epsilon P^{\frac{3}{2}} = (A/H^2)^{\frac{2}{3}}. \tag{88}$$

When substituting $\epsilon = (A/H^2)^{\frac{1}{4}}$ and $Q = \epsilon^{-\frac{3}{2}}A/H^2$, we also obtain

$$\epsilon P^{\frac{3}{2}} = (A/H^2)^{\frac{2}{3}}.$$

Therefore, by (86) and (87),

$$U_C(\epsilon = \alpha^{\frac{1}{2}}, Q = \epsilon^{-\frac{3}{2}}A/H^2) = U_C(\epsilon = (A/H^2)^{\frac{1}{4}}, Q = \epsilon^{-\frac{3}{2}}A/H^2),$$

$$U_L(\epsilon = \alpha^{\frac{1}{2}}, Q = \epsilon^{-\frac{3}{2}}A/H^2) = U_L(\epsilon = (A/H^2)^{\frac{1}{4}}, Q = \epsilon^{-\frac{3}{2}}A/H^2).$$

This completes the proof.

When $d = 1$ for the single-layer flow, the above formulae for U_C and U_L are reduced to

$$U_C/(gH)^{\frac{1}{2}} = 1 + \tfrac{1}{2}[9A/(4H^2)]^{\frac{2}{3}}, \tag{89}$$

$$U_L/(gH)^{\frac{1}{2}} = 1 - \tfrac{1}{2}[9A/(2H^2)]^{\frac{2}{3}}. \tag{90}$$

In the next subsection, we shall compare these two formulae with those first derived by Miles (1986) via another asymptotic approach called Rayleigh's formulation.

5.3. *Comparison of the results*

The comparison is conducted for the following five quantities: U_C, U_L, A_f, A_{s_h} and A_{s_l}. Here, U_C is the supercritical turning point, U_L the subcritical cutoff point, A_f the amplitude of the hydraulic fall, A_{s_h} the amplitude of the higher supercritical solitary wave, and A_{s_l} the amplitude of the lower solitary wave. U_C, U_L, A_f, A_{s_h} and A_{s_l} are dimensional quantities and physically observable. The experimental data are from Forbes (1988) and Sivakumaran *et al.* (1983). The computational data are from Vanden-Broeck (1987) and Forbes (1988, 1989).

5.3.1. *Single-layer flow forced by a semicircular bump*

Wu & Wu (1982) first conjectured the non-existence of transcritical stationary solutions by saying that 'The transcritical motion does not approach a steady state'. By Rayleigh's asymptotic formulation, Miles (1986) concluded that 'The hypothesis of steady flow presumably fails in the transcritical range'. This range, expressed in terms of the upstream Froude number, is (F_L, F_C). He found that

$$F_L = \left(1 - \left(\frac{9A}{2H^2}\right)^{\frac{2}{3}}\right)^{\frac{1}{2}}, \quad F_C = \left(1 + \left(\frac{9A}{4H^2}\right)^{\frac{2}{3}}\right)^{\frac{1}{2}}. \tag{91}$$

When A/H^2 is very small (i.e. the bump area is much smaller than that of the square $[0, H] \times [0, H]$), the linear approximation of (91) leads to the result in this paper (see (90) and (89)). Figure 10 presents the complete comparison among the asymptotic results by Miles (1986) and Shen (1991) and this paper, computational results by Vanden-Broeck (1987) and Forbes (1988), and the experimental results by Forbes (1988). One can see that the results from our approach are in reasonable agreement with those from the computational and experimental approach in the entire range of 'small' forcing. This agreement is the best in the range
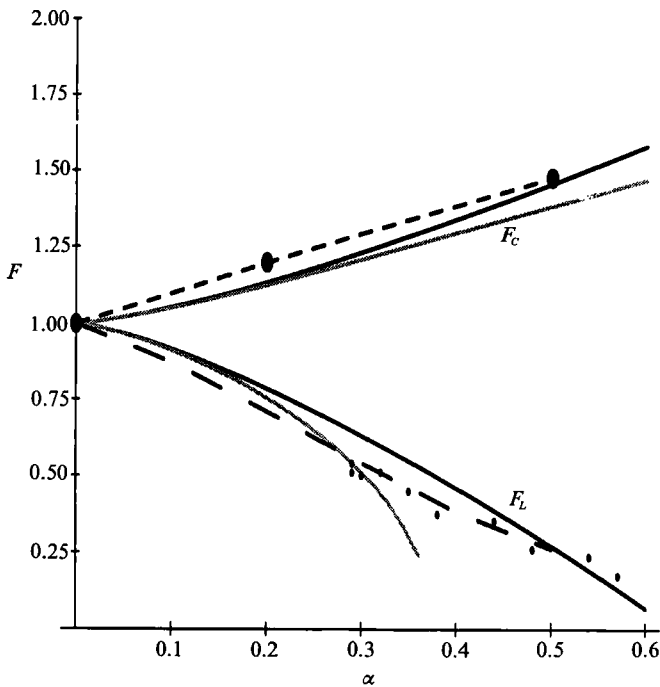
FIGURE 10. Comparison of the values of U_C and U_L in a single-layer flow over a semicircular bump of radius R. $\alpha = R/H$, where H is the depth of the flow. The solid lines represent the results from the fKdV (see (89) and (90)), the big dots Vanden-Broeck's (1987) computational results, the small dots Forbes' (1988) experimental results, the long dashed line Forbes' (1988) computational results, and the light lines Miles' (1986) asymptotic results.

	F_C			F_L		
α	Miles	Vanden-Broeck	Shen	Miles	Forbes	Shen
0.1	1.0525		1.0585	0.9105	0.87	0.9145
0.2	1.1276	1.2	1.1357	0.7545	0.71	0.7846
0.3	1.2108		1.2330	0.5102	0.54	0.6302
0.4	1.2976		1.3419		0.38	0.4572
0.5	1.3859	1.46	1.4604		0.26	0.2692

TABLE 1. Comparison of the values of the supercritical turning point Froude number and the subcritical cutoff point Froude number obtained by Miles (1986), Vanden-Broeck (1987), Forbes (1988) and Shen (the present paper)

$0.45 < \alpha < 0.55$ and the worst in the range $0.2 < \alpha < 0.4$. Miles' asymptotic procedure yields a very good result when $\alpha = 0.29$. But it seems that Miles' approach ceases to be valid when the forcing is strong, say $\alpha > 0.30$.

At $\alpha = 0.5$, Vanden-Broeck's computational approach yields $U_C/(gH)^{\frac{1}{2}} = 1.46$. We obtained the same value from our asymptotic approach. Also at $\alpha = 0.5$, Forbes' computational approach results in $U_L/(gH)^{\frac{1}{2}} = 0.26$. We obtained 0.27 from our asymptotic approach. The difference is about 4%. For a more detailed comparison of the values, see table 1.

Table 1 displays the computational results and asymptotic results for the upstream velocities U_C and U_L for $\alpha = 0.1, 0.2, 0.3, 0.4$ and 0.5. There are no

computational results available for $\alpha > 0.5$. According to (89) and (90), and the conservation of the flow flux, the ratio of the downstream velocity to the upstream velocity is extremely large when α is greater than 0.5. The large velocity ratio may contribute significantly to the flow instability. Probably, the phenomenon that the downstream cnoidal wave approaches a half-solitary wave (the tale of the hydraulic fall) as F increases to F_L, may disappear. Instead, a sharp-angle stagnation point on the free surface may appear in the supercritical region of the forcing site. This possibility was noticed by Forbes (1988). He described his opinion regarding this question from both numerical and physical viewpoints. Numerically, when $\alpha > 0.5$, the downstream velocity is very large and causes the numerical grid points to cluster very close together in the downstream portion of the flow. Hence, the numerical scheme fails to converge. Physically, he pointed out that the problem may become unstable when α is large (say, $\alpha > 0.5$). Perhaps, the transition state from the stable steady flow to the unstable flow is the appearance of a free-surface sharp angle on the site of forcing.

Recall that we assumed that the forcing is small (of order ϵ^2). However, as shown by comparison with the computational results and the experimental results, our approach is still valid even if the height of the circular bump is as large as half of the upstream depth. For this large forcing, the value of the 'small' number ϵ is now as large as 0.7.

Also recall our remark in §1 that the 'near'-critical assumption does not preclude reasonably large intervals, within which our asymptotic results are still valid. One can see from figure 10 that this 'near'-critical interval can be as large as $(0.26, 1.46)$ $(gH)^{\frac{1}{2}}$. This interval includes the critical speed $(gH)^{\frac{1}{2}}$. If the upstream depth H is equal to 0.5 m, then our 'near'-critical interval is $(0.57, 3.23)$ m/s $= (2, 12)$ km/h. This simple example shows that our asymptotic analysis is valid in a large range of flow speed and is applicable to most cases in practical applications.

Next, we compare the amplitudes of the solitary waves. Recalling the proof of Theorem 2, $Q\epsilon^{\frac{3}{2}} = A/H^2$ and $P = \frac{1}{2}Q$. From (67), we can get the relationship between the Froude number and the amplitudes of the higher and lower solitary waves:

$$\frac{\|\eta_s^{(1)*}\|_\infty}{H} = -\frac{A}{4H^2}\left(\frac{-3}{\bar{m}m_4(F-1)}\right)^{\frac{1}{2}}\left(\cos\left[\frac{1}{3}\arccos\left(\frac{-\sqrt{3}Am_3}{8H^2(-m_4\bar{m}^3(F-1)^3)^{\frac{1}{2}}}\right) + \left\{\begin{matrix}\frac{4}{3}\pi\\\frac{2}{3}\pi\end{matrix}\right\}\right]\right)^{-1}. \quad (92)$$

The phase shifts $\frac{4}{3}\pi$ and $\frac{2}{3}\pi$ correspond to the higher solitary wave amplitude A_{s_h} and the lower solitary wave amplitude A_{s_l} respectively. As $F \to \infty$, the angle

$$\theta = \frac{1}{3}\arccos\left(\frac{-\sqrt{3}Am_3}{8H^2(-m_4\bar{m}^3(F-1)^3)^{\frac{1}{2}}}\right) \to \frac{1}{6}\pi - 0.$$

For the lower branch, $\cos(\frac{1}{6}\pi + \frac{2}{3}\pi) = -\frac{1}{2}\sqrt{3}$. So A_{s_l} has a parabolic asymptote:

$$A_{s_l} \sim \frac{A}{2H(\bar{m}m_4(1-F))^{\frac{1}{2}}} \quad \text{as} \quad F \to \infty. \quad (93)$$

For the higher branch, we need to notice that if $x = \frac{3}{2}\pi - y$ and $y \sim 0+$, then $\cos x \sim -y$. One then can find a straight line asymptote for A_{s_h}

$$A_{s_h} \sim \frac{3\bar{m}(F-1)}{m_3}H \quad \text{as} \quad F \to \infty. \quad (94)$$

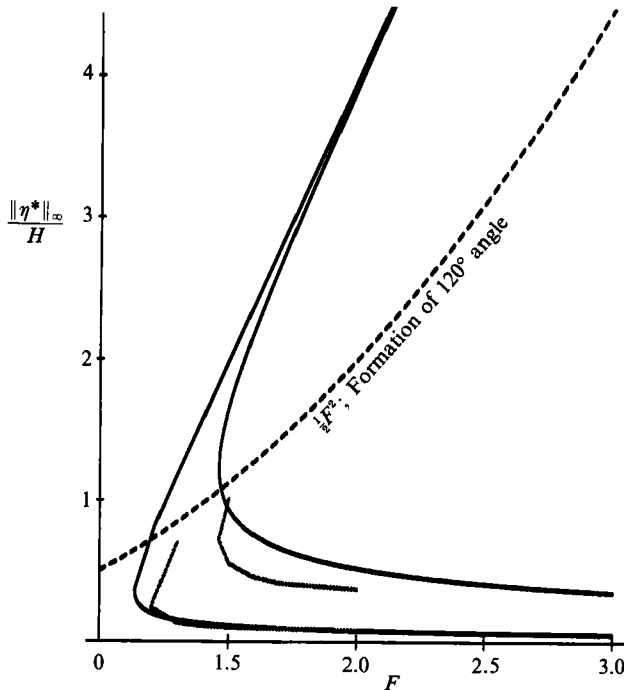This asymptote is independent of the magnitude of the forcing.

FIGURE 11. Comparison of supercritical turning point bifurcation for a semicircular bump of radius R. The solid lines represent the results from (92) in the present paper. The dotted lines represent Vanden-Broeck's (1987) computational results.

The turning point of the bifurcation diagram (i.e. the joining point of the A_{s_h} curve and the A_{s_1} curve) occurs at $\theta = 0$. This leads to

$$\frac{-\sqrt{3}A m_3}{8A(-m_4 \bar{m}^3 (F-1)^3)^{\frac{1}{2}}} = 1.$$

In turn, this leads to the value of the Froude number at the turning point:

$$F_C = 1 + \frac{1}{\bar{m}}\left(\frac{3m_3^2}{-64m_4}\right)^{\frac{1}{3}}\left(\frac{A}{H^2}\right)^{\frac{2}{3}}. \tag{95}$$

When $m_3 = -\frac{3}{2}$, $m_4 = -\frac{1}{6}$ and $\bar{m} = 1$, (95) is reduced to (89). Figure 11 presents a comparison of our asymptotic results with the computational results by Vanden-Broeck (1987). For the lower branch of the solitary waves, the agreement is better. For smaller forcing (i.e. smaller α), the agreement is also better. This certainly is what one expects, for the asymptotic approach should work better for smaller forcings and flatter waves. It is known that for a supercritical flow in a channel of flat bottom the surface solitary wave gradually develops a 120° sharp-angle singularity as the upstream Froude number increases (see Hunter & Vanden-Broeck 1983; Vanden-Broeck 1987). The nonlinearity becomes stronger for the singularity than for the smooth solitary waves. When the 120° sharp-angle singularity appears, the surface is not in the range of 'relative flat'. This flatness is the very assumption upon which the weakly nonlinear shallow-water theory is based. Therefore, when the 120° singularity occurs, the wave is no longer 'shallow'. Instead it is so 'deep' around the singularity that the surface does not feel the existence of the bottom. Viewing the

fluid is infinitely deep around the singularity, one can analytically find the structure of the 120° singularity (see any advanced fluid mechanics textbook). Dias & Vanden-Broeck (1989) showed that the same 120° singularity occurs for nonlinear surface waves forced by a bump in a single-layer flow. At the tip of the 120° angle, the flow speed is equal to zero. Bernoulli's equation results in the relationship between the amplitude of the wave (i.e. the elevation of the tip of the 120° angle) and the upstream Froude number F:

$$\eta^*/H = \tfrac{1}{2}F^2. \tag{96}$$

The dashed line in figure 11 corresponds to the above relation. The higher branch of solitary waves from asymptotics becomes invalid (at least physically) at the intersection with the dashed line. Compared with the results of Hunter & Vanden-Broeck (1983), the asymptotic solution of the upper branch solitary waves ceases to be valid before the intersection. For instance, in the case of zero forcing, the intersection is at $F = 2$, whereas the highest solitary wave occurs at the largest possible value of $F = 1.29091$. When forcing is present, these two values get closer. In any case, those points which are above the dashed line on the bifurcation diagram do not have physical counterparts. From figure 11, we see that the range for existence of the higher solitary wave is very short. This range is even shorter for stronger forcing. It is because of this short range of Froude number that it is difficult to conduct the experiment to observe stationary solitary waves.

Finally we come to the comparison of the amplitude of the hydraulic falls. From (80), one can get the amplitude of the hydraulic fall in the laboratory:

$$A_f = \left(\frac{3}{2m_3 m_4}\right)^{\frac{1}{3}}\left(\frac{A}{H^2}\right)H. \tag{97}$$

Let H_{DS} denote the downstream depth of the hydraulic fall. Then

$$\frac{H_{\mathrm{DS}}}{H} = 1 - \left(\frac{3}{2m_3 m_4}\right)^{\frac{1}{3}}\frac{A}{H^2}. \tag{98}$$

This relation is plotted in figure 12. The computational results and experimental results due to Forbes (1988) are included in the figure for comparison. The agreement is best when α is near 0.45.

The concavity of the curves in figure 12 seems deserving of further attention. Our asymptotic approach gives a concave down curve, whereas both computational and experimental results due to Forbes support a concave up relation when α is larger than 0.1. This disagreement remains to be clarified.

5.3.2. *Single-layer flow forced by a Gaussian bump*

Sivakumaran *et al.* (1983) experimentally determined hydraulic fall profiles over a Gaussian bump. The shape of the bump is given by $y^* = 20\exp(-\tfrac{1}{2}(x^*/24)^2)$ cm. Hence the area of the bump is $A = 240(2\pi)^{\frac{1}{2}}$ cm^2. In their figure 7(a), the upstream depth is $H = 34.8$ cm, and the upstream Froude number is 0.17. By our formula (90), it is found that $F_L = 0.15$, which is about 10% below the experimental value 0.17. This is consistent with our previous comparison with Forbes' results. Namely, when $\epsilon > 0.7$, our asymptotic formula (90) will underestimate the upstream Froude number F_L. Part of this error is contributed by the δ-function approximation of the bump. For a big bump, the base of the bump is no longer much smaller than the height after the non-dimensionalization since $\epsilon^{\frac{1}{3}}$ is no longer small. Hence the δ-
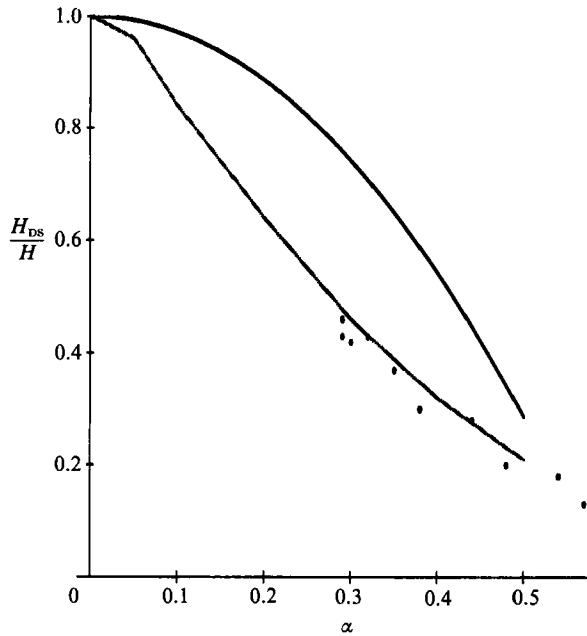
FIGURE 12. Comparison of the downstream depth after the subcritical hydraulic fall with Forbes' results. The solid line is the results from (98) in the present paper. The light line represents Forbes' (1988) computational results and the dots represent Forbes' (1988) experimental results.

function approximation would introduce a noticeable error. In addition, we have seen that the δ-function approximation does not distinguish the shape of the bump. Instead it basically regards every bump as a short obstruction of the same area. The shorter the obstruction, the better the approximation. Intuition suggests that the hydraulic fall over a shorter bump of the same area corresponds to a lower upstream velocity. Hence our formula (90) would underestimate the upstream velocity of a hydraulic fall. In the example above, $\epsilon = (20/34.8)^{\frac{1}{2}} = 0.76 > 0.7$. After the non-dimensionalization the bump is not short enough. Consequently, our formula (90) underestimates F_L and does not yield an accurate answer.

When the δ-function approximation fails, one has to use some numerical methods to solve the boundary-value problem for the fKdV. A numerical scheme for finding solitary waves from the fKDV has been given in §3. Direct integration from the Laplace equation for finding hydraulic falls over a Gaussian bump was done by King & Blohr (1990). Numerical methods for finding hydraulic falls from the fKdV can be found in Shen & Shen (1990).

In figure 7(b) of Sivakumaran *et al.* (1983), the upstream depth is $H = 27.2$, and the upstream Froude number is 0.81. Now $\epsilon = (20/27.2)^{\frac{1}{2}} = 0.86$. This ϵ is too big to be considered as a small number in our asymptotic procedure. This is basically because of the reason stated above concerning the δ-function approximation. Fortunately, there exist other types of asymptotic approaches which can be used to find those wave free surfaces over large bumps. These approaches are called the Saint-Venant method and the Green-Naghdi method, respectively. For details, see Sivakumaran *et al.* (1983) and Naghdi & Vongsarnpigoon (1986).

5.3.3. *Two-layer hydraulic falls over a semicircular bump*

The comparison here is with the recent computational results due to Forbes (1989). He considered the hydraulic falls of two-layer flows over a semicircular bump in a two-dimensional channel. We will see that his results apply only for the fast mode. This is not surprising, because for the examples he presented, the slow-mode hydraulic falls correspond to either rest water or backflow.

In his figure 1, $\sigma = 1$, $\rho = 0.6$, $\gamma = 1.454$, and $\alpha = 0.45$. For the fast mode, by the formulae derived in §2 we have $c_i^{(0)} = 1.154$, $c_s^{(0)} = 1.003$, $m_1 = 1.706$, $\bar{m} = 1.869$, $m_3 = -1.824$, $m_4 = -1.497$. Then, the upstream velocity of the internal layer can be computed by following the method in §5.3.1. The result is $c_i(gH_1)^{\frac{1}{2}} = (c_i^{(0)} + \epsilon\lambda_L)(gH_1)^{\frac{1}{2}} = 1.006(gH_1)^{\frac{1}{2}}$. Forbes' computational result is $1.0(gH_1)^{\frac{1}{2}}$. This may be regarded as an exact agreement.

For the slow mode, also by the formulae derived in §2, we have $c_i^{(0)} = 0.377$, $c_s^{(0)} = 0.548$, $m_1 = 1.708$, $\bar{m} = 2.205$, $m_3 = -2.187$, $m_4 = -0.062$. The upstream velocity of the internal layer is $c_i(gH_1)^{\frac{1}{2}} = -0.031(gH_1)^{\frac{1}{2}}$. This may be regarded as rest water.

The dashed lines in Forbes' figure 4 correspond to: $\sigma = 0.4$, $\rho = 0.6$, $\gamma = 1.0$, and $\alpha = 0.2$. For the fast mode, we have $c_i^{(0)} = c_s^{(0)} = 1.129$, $m_1 = \bar{m} = 0.890$, $m_3 = -1.069$, $m_4 = -0.268$. Then the upstream velocity of the internal layer is $c_i(gH_1)^{\frac{1}{2}} = 0.998(gH_1)^{\frac{1}{2}}$. Forbes' result is $1.0(gH_1)^{\frac{1}{2}}$. This is an exact agreement too. Actually, Forbes proceeded differently in his computation. He prescribed the upstream velocity of the internal layer and regarded the depth of the surface layer as the unknown. That is, he assumed $c_i^{(0)} = 1$ and used this to find the unknown σ. In the present asymptotic formulation, we see from (38) that one can find any one of the five quantities σ, ρ, α, γ, and c_i as long as the other four are prescribed.

For the slow mode of the above example, we found that $c_i = -0.270$. This corresponds to a backflow hydraulic fall.

For the solid lines in Forbes' figure 4, $\sigma = 0.4$, $\rho = 0.6$, $\gamma = 1.0$, and $\alpha = 0.425$. We found that $c_i = 0.727$. This is very much below Forbes' computational result 1.0. Probably, this is because the base of the bump is too long for our δ-function approximation to be valid.

6. Discussion and concluding remarks

In this section, we first discuss the following two issues: transcritical solutions of the fKdV and the critical layers. Then we make some concluding general remarks about forced two-layer flows.

Recall that the upstream velocity is called transcritical if $\lambda_L < \lambda < \lambda_C$. Transcritical upstream soliton radiation solutions of fKdV have been studied by many authors since 1982. All of the studies have confirmed the original numerical and experimental discoveries made by Professor T. Yao-Tsu Wu's group in Caltech (Wu & Wu 1982; Huang *et al.* 1982). This group investigated the forced single-layer flow. They found that when the upstream velocity is near the shallow-water critical velocity $(gH)^{\frac{1}{2}}$, the flow never approaches a steady state 'in conspicuous contrast to the steadiness of a moving disturbance'. Instead, solitons are periodically generated at the site of the disturbance and radiated upstream. Immediately behind the disturbance a region of depressed water with almost uniform depth appears. The downstream end of the region of depressed water propagates downstream at a uniform speed. The surface of the downstream water following this depressed water region consists of a section of a tampering wake, which becomes weaker further

downstream. The length of this wake section grows uniformly with time. Wu's group has supported their finding by experiments, the Boussinesq theory and the fKdV theory. From different perspectives, Cole (1985), Mei (1986), Grimshaw & Smyth (1986), Smyth (1987), Wu (1987) and Lee *et al.* (1989) made their contributions to support the upstream soliton radiation phenomenon. Wu (1987) was very much concerned with an analytical expression of the period of the soliton generation. From the fKdV, he derived an approximate formula for this period. Nevertheless, this formula requires knowledge of the downstream depression, but this downstream depression is supposed to be an unknown. The beauty of Wu's derivation lies in its simplicity and clear physical meaning. Smyth (1987) found an approximate formula for this period from the modulation theory for the KdV. This formula yields results which agree well with numerical solutions of the fKdV.

The formulae due to Wu (1987) and Smyth (1987) both fail to predict the correct soliton generation period when λ is in (λ_L, λ_C) but close to the boundary points. Actually, whether the maximum soliton radiation range of the upstream velocity is (λ_L, λ_C) is still an unanswered question (Shen 1991). Lee *et al.* (1989) tried to provide an answer to the question from a numerical viewpoint, but they could not reach a clear conclusion.

Stationary solutions exist when $\lambda \geqslant \lambda_C$ and $\lambda \leqslant \lambda_L$. Some of these solutions have been conjectured to be stable (Shen 1989). The surface elevation tends to be sustained on the site of forcing and downstream for $\lambda > \lambda_C$ and $\lambda < \lambda_L$ respectively. Hence, it seems that when λ is in (λ_L, λ_C) but close to the boundary points, the soliton first generated is trapped at the site of the forcing and needs a long time to be radiated upstream. When $\lambda = \lambda_L$ or $\lambda = \lambda_C$, this 'long time' becomes infinity and the soliton radiation episode disappears. Consequently, the flow approaches a stable steady state and remains in this state later on.

Next we discuss the critical layers. From §§3 and 4, the amplitude of the solitary wave and that of the hydraulic fall are inversely proportional to the coefficient m_4 of the fKdV. However m_4 can be zero for some parameters. When ρ, γ and the forcing are fixed, the solution of $m_4(\sigma) = 0$ gives the critical thickness ratio σ_C. The interface of the two fluids with the critical thickness ratio σ_C is called the critical layer. In this case, our asymptotic method fails because our approach yields unbounded solutions. The reason is that the nonlinearity in the critical-layer flow is too strong to be described by the fKdV. The free boundary response to forcing of order ϵ^2 is larger than order ϵ. Recall the Miura transformation from the standard KdV to the modified KdV:

$$u_t - 6uu_x + u_{xxx} = 0 \quad \text{(standard KdV)},$$

$$u = v^2 + v_x \quad \text{(Miura transformation)},$$

$$\left(2v + \frac{\partial}{\partial x}\right)(v_t - 6v^2 v_x + v_{xxx}) = 0 \quad \text{(transformed equation)},$$

$$v_t - 6v^2 v_x + v_{xxx} = 0 \quad \text{(modified KdV as a first integral)}.$$

One can see that if $u(x, t)$ is of order ϵ, then $v(x, t)$ is of order $\epsilon^{\frac{1}{2}}$. Hence we may assume the order of the stronger nonlinear response is $\epsilon^{\frac{1}{2}}$. This idea was used by Kakutani & Yamasaki (1978). However, we have a great difficulty here. Because of the forcing, the inhomogeneity of the fKdV prevents the transformed equation from having an obvious first integral as given above for the KdV. In the case of the critical layer, the asymptotically reduced equation is a fourth-order partial differential equation, which is generally more difficult to solve.

Finally, we briefly summarize our present paper and make some remarks about future studies in this area. It has been shown that the fKdV type of asymptotic method is an effective approach to study long waves in single-layer and two-layer flows over a bump. When the support of the bump is less than the depth of the internal layer, the bump may be regarded as local and approximated by the Dirac delta function. With this approximation, all the supercritical and subcritical waves can be analytically found. The error due to this δ-function approximation should be small. Otherwise, the Dirac delta function approximation may sometimes result in a large error and the bump should now be regarded as non-local. In that case, numerical methods are required to solve the non-locally forced fKdV. The analytical solutions for a local bump make the results, which otherwise need numerical solutions, more transparent. However we emphasize again that this Dirac delta function approximation fails when the support of the bump is long. The long bump belongs to the category of non-local forcing and a numerical method must be employed to solve the fKdV.

There remain many interesting and important problems to solve. We list three of them here. First, under what lengthscale of the waves does the free-surface elevation couple with the interface elevation in algebraic order less than 4? In that case, what would be the classification of the solutions according to the upstream velocity? The second problem concerns the critical layer. In critical-layer flows, can one recover the dispersive and non-dissipative internal bore observed by Melville & Helfrich (1987)? The third is a big and very difficult mathematical problem. Can one find an inverse scattering method or a nonlinear superposition principle of Bäcklund type of transformation for the fKdV? The difficulty lies in the disappearance of the symmetry which is associated with an unforced KdV. The Lie group method cannot be directly applied to the inhomogeneous fKdV. Establishment of a theory to find analytical solutions to inhomogeneous evolution equations would be a significant contribution to mathematics and physics. Fokas & Ablowitz (1989) have already made a first try.

REFERENCES

BAINES, P. G. 1984 A unified description of two-layer flow over topography. *J. Fluid Mech.* **140**, 127–167.

BAINES, P. G. 1987 Upstream blocking and airflow over mountains. *Ann. Rev. Fluid Mech.* **19**, 75–97.

BENJAMIN, T. B. & LIGHTHILL, M. J. 1954 On cnoidal waves and bores. *Proc. R. Soc. Lond.* A **224**, 448–460.

COLE, S. L. 1985 Transient waves produced by flow past a bump. *Wave Motion* **7**, 579–587.

DIAS, F. & VANDEN-BROECK, J.-M. 1989 Open channel flows with submerged obstructions. *J. Fluid Mech.* **206**, 155–170.

FOKAS, A. S. & ABLOWITZ, M. J. 1989 Forced nonlinear evolution equations and the inverse scattering transform. *Stud. Appl. Maths* **80**, 253–272.

FORBES, L. K. 1988 Critical free-surface flow over a semi-circular obstruction. *J. Engng Maths* **22**, 3–13.

FORBES, L. K. 1989 Two-layer critical flow over a semi-circular obstruction. *J. Engng Maths* **23**, 325–342.

FORBES, L. K. & SCHWARTZ, L. W. 1982 Free-surface flow over a semi-circular obstruction. *J. Fluid Mech.* **114**, 299–314.

GRIMSHAW, R. H. J. & SMYTH, N. 1986 Resonant flow of a stratified fluid over topography. *J. Fluid Mech.* **169**, 429–464.

HUANG, D. B., SIBUL, O. J., WEBSTER, W. C., WEHAUSEN, J. V., WU, D. M. & WU, T. Y. 1982 Ships moving in the transcritical range. In *Proc. Conf. on Behavior of Ships in Restricted Waters, Varna*, Vol. 2, pp. 26/1–26/10. Bulgarian Ship Hydrodynamics Center.

HUNTER, J. K. & VANDEN-BROECK, J.-M. 1983 Accurate computations for steep solitary waves. *J. Fluid Mech.* **136**, 63–71.

KAKUTANI, T. & YAMASAKI, N. 1978 Solitary waves on a two-layer fluid. *J. Phys. Soc. Japan* **45**, 674–679.

KING, A. C. & BLOHR, M. I. G. 1987 Free surface flow over a step. *J. Fluid Mech.* **182**, 193–208.

KING, A. C. & BLOHR, M. I. G. 1990 Free streamline flow over curved topography. *Q. Appl. Maths* **48**, 281–293.

LEE, S. J., YATES, G. T. & WU, T. Y. 1989 Experiments and analyses of upstream-advancing solitary waves generated by moving disturbances. *J. Fluid Mech.* **199**, 569–593.

MEI, C. C. 1986 Radiation of solitons by slender bodies advancing in a shallow channel. *J. Fluid Mech.* **162**, 53–67.

MELVILLE, W. K. & HELFRICH, K. R. 1987 Transcritical two-layer flow over topography. *J. Fluid Mech.* **178**, 31–52.

MILES, J. W. 1986 Stationary, transcritical channel flow. *J. Fluid Mech.* **162**, 489–499.

NAGHDI, P. M. & VONGSARNPIGOON, L. 1986 The downstream flow beyond an obstacle. *J. Fluid Mech.* **162**, 223–236.

PATOINE, A. & WARN, T. 1982 The interaction of long, quasi-stationary baroclinic waves with topography. *J. Atmos. Sci.* **39**, 1018–1025.

PETERS, A. S. & STOKER, J. J. 1960 Solitary waves in liquids having non-constant density. *Commun. Pure Appl. Maths* **13**, 115–164.

SHEN, S. S. P. 1989 Disturbed critical surface waves in a channel of arbitrary cross section. *Z. Angew. Math. Phys.* **40**, 216–229.

SHEN, S. S. P. 1991 Locally forced critical surface waves in channels of arbitrary cross sections. *Z. Angew. Math. Phys.* **42**, 122–128.

SHEN, S. S. P. & SHEN, M. C. 1990 A new equilibrium of subcritical flow over an obstruction in a channel of arbitrary cross section. *Eur. J. Mech.* B **9**, 59–74.

SIVAKUMARAN, N. S., TINGSANCHALI, T. & HOSKING, R. J. 1983 Steady shallow flow over curved beds. *J. Fluid Mech.* **128**, 469–487.

SMYTH, N. F. 1987 Modulation theory solution for resonant flow over topography. *Proc. R. Soc. Lond.* A **409**, 79–97.

VANDEN-BROECK, J.-M. 1987 Free-surface flow over a semi-circular obstruction in a channel. *Phys. Fluids* **30**, 2315–2317.

WU, D. M. & WU, T. Y. 1982 Three-dimensional nonlinear long waves due to moving surface pressure. In *Proc. 14th Symp. Naval Hydrodyn.*, pp. 103–125. Washington: National Academy of Sciences.

WU, T. Y. 1987 Generation of upstream advancing solitons by moving disturbances. *J. Fluid Mech.* **184**, 75–90.

YIH, C. S. 1979 *Fluid Mechanics*. Ann Arbor: West River Press.